© Copyright 2017

Eric A. Wheeler

Experimental Investigation of Throatless Supersonic Exhaust Velocity in a Rotating Detonation Engine

Eric A. Wheeler

A thesis
submitted in partial fulfillment of the
requirements for the degree of

Master of Science

University of Washington
2017

Committee:
Dr. Carl Knowlen
Dr. Mitsuru Kurosaka

Program Authorized to Offer Degree:
Aeronautics and Astronautics

University of Washington

Abstract

Experimental Investigation of Throatless Supersonic Exhaust Velocity

in a Rotating Detonation Engine

Eric A. Wheeler

Chair of the Supervisory Committee:
Dr. Carl Knowlen
Aeronautics and Astronautics

Generating supersonic exhaust without using converging-diverging geometry is an attractive feature desired in all propulsion devices that have supersonic flows. The inherent increased thermodynamic efficiency of combustion by detonation and supersonic azimuthal velocity of the detonation wave front both lend to a sense of curiosity about the possibility of supersonic axial exhaust velocity. Numerical simulations and some experiments have shown that there are oblique shock waves in the exhaust, which are inexorably linked to the detonation wave front. Do these phenomena create the necessary conditions for this to be possible? Experimental investigation into the exhaust characteristics of a rotating detonation engine have yielded very positive results and are discussed in this paper. Also, this engine features a unique injection method for fuel and oxidizer. While there has been some latent desire to explore the flow characteristics of the mixing zone ahead of detonation, aberrant pressure transducer readings on the front end wall of the combustor has been the catalyst into undertaking this task. The results of CFD analysis show possible explanations for this unusual behavior, along with possible explanations for additional effects of engine operation.

TABLE OF CONTENTS

Table of Contents iv

List of Figures vi

List of Tables viii

Nomenclature ix

Acknowledgments x

Chapter 1: Introduction 1

Part One

Chapter 2: Experimental Setup 4

2.1: Physical Layout 4

2.2: System Control, Data Collection, and Processing 7

2.3: Testing Procedure 9

2.4: Experimental Objectives 9

Chapter 3: Results and Discussion 10

3.1: A Brief Explanation of the Fourier Transform 10

3.2: Relationship Between the Normal Detonation Wavefront and Attached Oblique Shocks 11

3.3: Effect of Downstream Conditions on Combustor Pressures 13

3.4: Front End Wall Pressure Measurements 16

3.5: Measurement of Flow Mach Number and Effect of Expansion Nozzle 17

Chapter 4: Conclusions and Recommendations 21

Part Two

Chapter 5: Constructing the Model Domain 23

Chapter 6: Solver Setup 24

Chapter 7: Results and Discussion 29

7.1: Residuals Convergence Management 29

7.2: Pressure Contours 30

7.3: Vortical Entrainment of Fluids 32

7.4: Effect of Jet Impingement on Combustor Walls 34

Chapter 8: Conclusions and Recommendations 35

References 37

LIST OF FIGURES

Figure 1.1. CFD model of detonation wave traveling within an annular region 1

Figure 2.1. (a) Close-up photo of the installed UW RDE and (b) test rig with dump tank at the far right. 4

Figure 2.2. Butterfly valve (in blue) set upstream of dump tank.....4

Figure 2.3. Diagram of major elements of the experimental setup.....5

Figure 2.4. Fully assembled RDE with expansion nozzle 5

Figure 2.5. Pressure sensor arrangement in the RDE. Typical detonation zone is in yellow.....6

Figure 2.6. Placement of front end wall pressure taps and orientation of injector orifices 6

Figure 2.7. Block diagram of the system setup.....8

Figure 2.8. Current engine control sequence starting at t+1 seconds from user command. 8

Figure 2.9. Diagram of cold-side oblique shock pattern linked to the normal detonation waves ...9

Figure 3.1. Deconstruction of a time signal into the Fourier domain.....11

Figure 3.2. Frequency response spectrograms during engine operation with butterfly valve at (a) 5.5 and (b) 6.0.....12

Figure 3.3. Combustor end-wall pressures during cold-shot tests.....13

Figure 3.4 Combustor end wall pressures for all BFV settings during engine hot-fire.....14

Figure 3.5. Spectrogram of hot fire runs with BFV set at (a) 4.5 and (b) 5.5.....14

Figure 3.6. High-speed pressure transducer raw voltage for BFV set at (a) 4.5 and (b) 5.5 15

Figure 3.7. Combustor 1 and 2 sensor data during engine operation 16

Figure 3.8. Combustor pressures for (a) hot fire and (b) cold fire tests.....17

Figure 3.9. Flow Mach number, combustor pressures, and exhaust pressures for BFV setting of 4.5. 18

Figure 3.10. RDE flow time-averaged pathlines in the lab frame created by numerical simulation 19
Figure 3.11. Composite plot of combustor exit Mach numbers 20
Figure 3.12. Partially melted pitot tube used in the combustor region 21
Figure 5.1. Solidworks model cutaway of the UW RDE 23
Figure 5.2 Sketch of vortical entrainment due to staggered injector orifices 24
Figure 5.3. Volume extracted from one-eighth section of the RDE. The combustor has also been truncated 24
Figure 6.1. Standard mesh (above) compared to adapted mesh (below) 25
Figure 6.2. Experimental data used for model inputs of inlet mass flow rate 26
Figure 6.3. Experimental data used for (a) initial guesses for inlet pressure and (b) combustor sensor validation 27
Figure 7.1. Residuals and convergence criteria used to establish model validity 30
Figure 7.2. Pressure contours in the range of (a) 0 to 575 kPa and (b) 0 to 30 kPa 31
Figure 7.3. Engine sidewall pressure contour with possible sensor location outlined in black 31
Figure 7.4. Side views of (a) pressure contour and (b) velocity vectors on a plane bisecting an O2 injector orifice 32
Figure 7.5. Front view of 3D streamline plot 33
Figure 7.6. Comparison of predicted vortical entrainment with CFD model results 33
Figure 7.7. Sidewall and isometric views of 3D streamline plot 34
Figure 7.8. Combustor inner annulus wall after almost 100 engine hot-fires 35
Figure 7.9. Pressure isosurface bisecting a fuel injector orifice 35

LIST OF TABLES

Table 2.1. Pressure transducer model data..... 7

Table 2.2. Critical RDE dimensions 7

Table 2.3. Engine operation parameters 9

NOMENCLATURE

P_0	Total pressure
P	Static pressure
M	Mach number
γ	Specific heat ratio
$\dot{m}$	Mass flow
C_D	Discharge coefficient
A	Cross-sectional area
R	Specific gas constant
T_0	Total temperature

ACKNOWLEDGMENTS

Both Dr. Carl Knowlen and Dr. Mitsuru Kurosaka have provided countless hours of mentoring and stewardship over myself and my work in the lab. For that, they have an enormous amount of my gratitude. If ever I started to doubt myself, they were always there to give me the encouragement I needed. Every time I needed to talk, the door was always open. If I needed a kick in the pants– Well… you know how it goes. I will miss the almost daily impromptu meetings in the office, where we could banter back and forth over how to tackle a problem or discuss the most recent results from an experiment, and then smoothly segue into non-engineering chit-chat. It was this cycle that helped me keep my chin up and learn how to beat that ever-looming presence of Impostor Syndrome. Thanks for everything.

I'd also like to acknowledge my family and friends, without whose support and interactions, my psychological health might have been worse off. They were there to listen when I needed to vent my frustrations and were also there when I just had to get out of the lab to go get a burger and fries for lunch.

Finally, the greatest gratitude of all goes to my girlfriend, Bonnie. Her love and support have remained with me at all times, good or bad. It was this omnipresence that kept me charging ahead, no matter what. She's been with me all these years, waiting for me to finally finish school. That time is nigh… the time where we can finally take a huge step forward in our lives together. Bonnie, I've learned over these past few years that I can always look to my side and know that you'll still be there. I look forward to the many, crazy adventures that we will share in the future.

CHAPTER 1: INTRODUCTION

In all propulsion systems that utilize supersonic flow of a fluid, there must be the inclusion of a converging-diverging nozzle in order to transition the high-pressure subsonic flow into low-pressure supersonic flow. This geometry, while effective in its purpose, also presents a challenging design consideration: how to handle the massive levels of heat flux being forced through the walls of the throat. Various cooling designs have been implemented to offset this detrimental effect in rocket engines, but their inclusion adds to the overall complexity and mass of the structure. The rotating detonation engine (RDE) offers a possible solution to this problem.

As its name implies, the RDE utilizes detonation waves to compress and combust fuel and oxidizer. These waves travel circumferentially in an annular combustor region within the engine and continues to propagate without external ignition, as long as mixed fuel and oxidizer are supplied at the necessary flow rates. The entire process is more thermodynamically efficient than conventional deflagration, or subsonic combustion, of reactants[1].

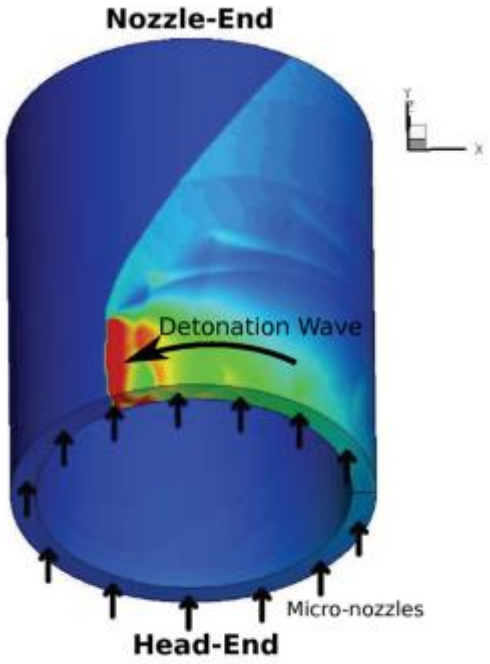

Figure 1.1. CFD model of detonation wave traveling within an annular region[i]

The development and research of the RDE has come far in the last couple of decades, showing several areas in which it can surpass and/or augment some current propulsion systems. One such area of improvement is the possibility of the RDE to be able to deliver supersonic exhaust without the need for converging-diverging geometry, thus possibly eliminating the need for additional cooling. This relatively new propulsion device

promises the same, or greater, performance while offering significant weight savings in multiple ways.

There are several possible mechanisms, or combination thereof, that can generate this supersonic flow. The massive pressure spike inherent in the detonation wave acts as a driving force for the local fluids, imparting a significant momentum upon them as it sweeps by. In the detonation wave reference frame, this can be analogized as water flowing down a steep surface such as a dam overflow spillway. The more obvious contributor is the enormous heat release after the detonation of the fuel and oxidizer. The increased thermodynamic efficiency of detonation provides more useful energy to accelerate the flow away from the larger pressure gradients. Numerical modeling in the shock reference frame shows relatively high absolute Mach numbers in flows local to the detonation wave front. These magnitudes, along with the requirement for the fluid to relax and expand towards low pressure areas downstream, can possibly lead to supersonic velocity in the axial direction[2].

One of the many phenomena occurring on the inside of the RDE during operation is the formation and propagation of oblique shockwaves attached to the normal detonation wave. An oblique shock exists on both the cold side (upstream of the detonation zone), and the hot side (combusted and expanding gases downstream). While these two oblique shocks have differing characteristics, their existence has been largely supposed. Using newly installed pressure taps on the front end wall of the engine, the cold-side oblique shock frequency can be detected and linked to the frequency of the normal detonation wave(s) that exist in the engine during operation.

Also, the length of the RDE's combustor is largely dependent on the mixing quality upstream from the detonation zone. Some designs get around this by premixing fuel and oxidizer before entry into the combustor annulus. Otherwise, the injection method is crucial in determining this

effectiveness. Injector designs for this type of engine in many other research facilities involves some form of axial injection, often using one jet to impinge directly onto each other for mixing purposes. The University of Washington's RDE uses a unique configuration that has zero axial inlet velocity, instead choosing to inject radially using staggered orifices. The objective is to allow the jets to impinge onto the opposing wall in the combustor, instead of directly into each other. This should cause vortical entrainment of the fuel and oxidizer, promoting more effective mixing prior to reaching the detonation zone.

This paper will effectively be split into two parts. Part One will describe the experimental verification or invalidation of the presence of throatless supersonic exhaust velocity. Part Two will show the results of injector and combustor flow simulations using computational fluid dynamics (CFD), with accompanying discussion.

Part One
Experimental Data from Engine Operation

CHAPTER 2: EXPERIMENTAL SETUP

2.1: PHYSICAL LAYOUT

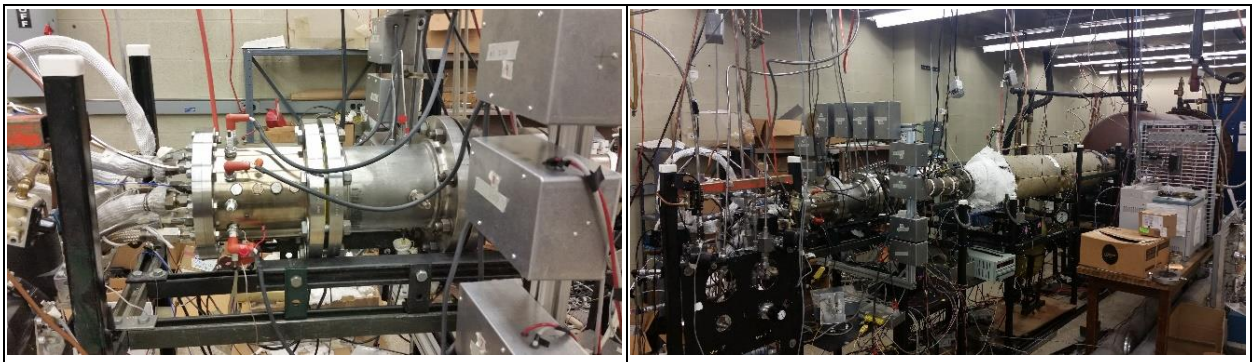

(a) (b)

Figure 2.1. (a) Close-up photo of the installed UW RDE and (b) test rig with dump tank at the far right.

Figure 2.1a shows a close-up of the physical engine. The plumbing to the left consists of oxidizer and fuel inlets, along with instrumentation to measure pressure and temperature of the inlet manifolds and combustor front end wall. The spark plug arrangement is part of the UW's Wave Generator ignition system, which is discussed in considerable detail in [3]. For these experiments, only 6 plugs are used. This configuration is shown to be just as reliable as the original configuration of 12 plugs. Further downstream, a 6" I.D. spool houses

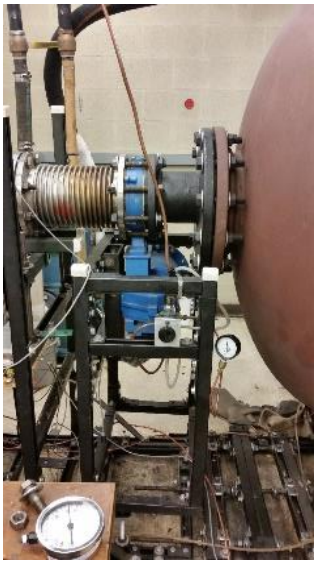

Figure 2.2. Butterfly valve (in blue) set upstream of dump tank

a static pressure probe at bottom, along with a total pressure probe at top.

Figure 2.1b shows the entire testing rig, which is a sealed system capable of drawing down the ambient pressure for near-vacuum operation of the engine. In the background on the right is the dump tank, which is preceded by a pressure-actuated butterfly valve (BFV).

The deflection value of this valve will be varied during the experiment to affect a change in system back pressure. By setting a lower pressure to the actuator, the BFV will be in a more closed state, and vice-versa.

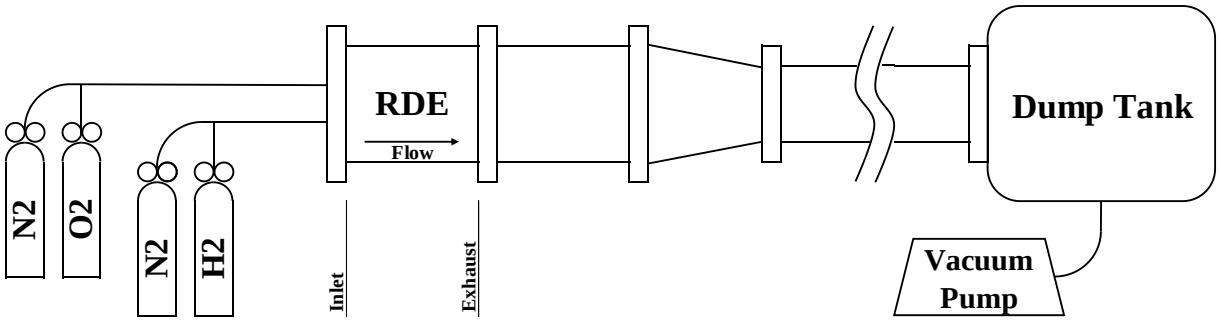

Figure 2.3. Diagram of major elements of the experimental setup

Fuel and oxidizer are delivered by pressurized cylinders of gas, which are controlled by a series of pneumatically actuated valves and manual regulators. N2 gas is used for pre- and post-purge activity, while the engine itself runs on gaseous H2 and O2. Venturi flow meters measure flow rate for each individual inlet line. Engine exhaust flows into the high volume dump tank and is pumped out in between engine firings.

Some recent modifications were made to the RDE in order to facilitate the investigation into the existence of supersonic exhaust. First, there was the addition of a constant-slope expansion nozzle to the end of the combustor, seen in Figure 2.4. The

Figure 2.4. Fully assembled RDE with expansion nozzle

nozzle has a constant-slope conical form that reduces from the inner annulus diameter of 5.18 inches to approximately 0.75 inches over a length of 5.9 inches. This translates to a declination of approximately 23 degrees. Its design is not optimized for thrust contribution; it is merely intended as a proof-of-concept to further accelerate supersonic velocity after the combustor. Of course, this will only be achieved if the exhaust is supersonic before reaching the nozzle.

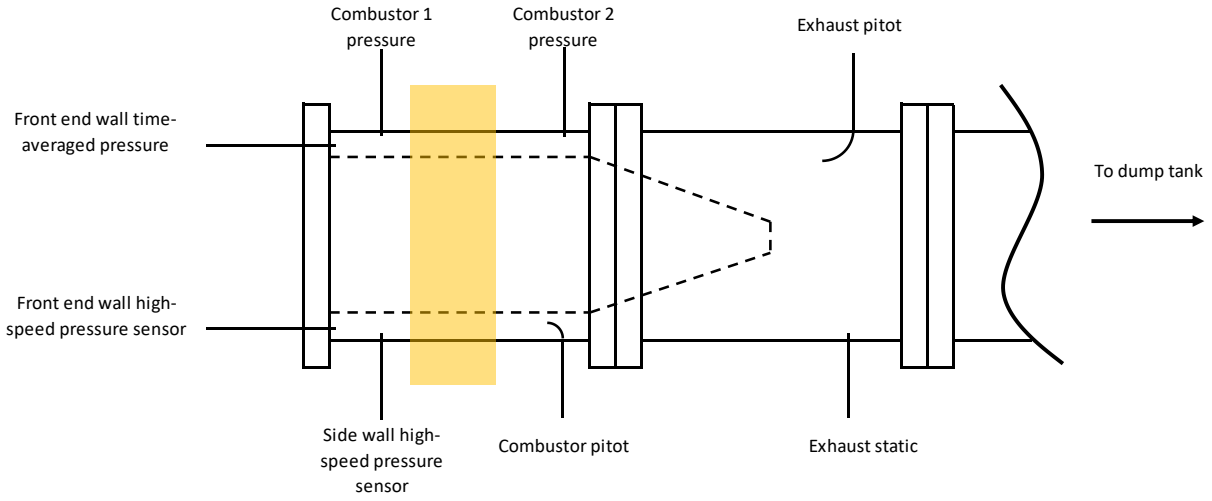

Figure 2.5. Pressure sensor arrangement in the RDE. Typical detonation zone is in yellow.

In order to observe the nozzle's effect on the exhaust, two pairs of pitot tube and static pressure stations were installed. One pair was inserted into the end of the engine combustor, while the other was placed in the exhaust section downstream.

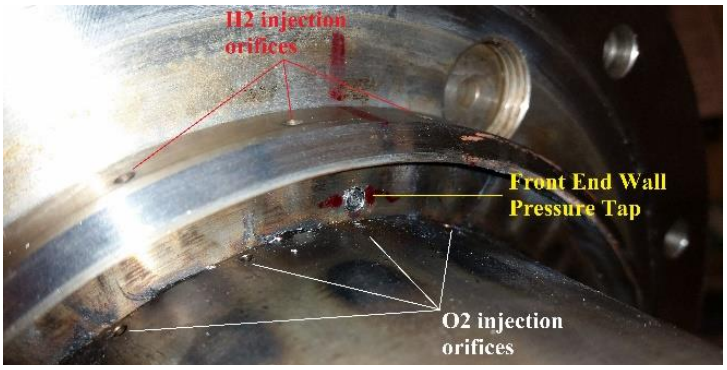

Figure 2.6. Placement of front end wall pressure taps and orientation of injector orifices

Another major change was the addition of two pressure taps at the engine front wall, one of which is shown in Figure 2.6. This will allow crucial time-averaged and high speed pressure data to be gathered for

analysis. Both taps are located directly above an O2 injection orifice. One of the objectives for this modification is to observe any effect, or lack thereof, on the combustor pressures due to changes in back pressure. This will help confirm or deny the existence of supersonic flow in the engine's current configuration which, again, does not feature a geometrical throat.

Also, take notice of the staggered arrangement of the H2 (marked in red) and O2 (marked in white) injection orifices. The effects of this design will be simulated and discussed in Part Two of this paper.

Table 2.1. Pressure transducer model data

Sensor	**Manufacturer**	**Model**
High speed pressure transducers	PCB Piezotronics	112-A05, 113-B22
Manifold pressures	Omega Engineering	PX319-1KG5V
Venturi flow meter pressures	Omega Engineering	PX319-500G5V
Combustor, exhaust pressures	Honeywell	19C050PA4K

Table 2.2. Critical RDE dimensions

Centerline diameter	14.28 cm
Outer annulus diameter	15.40 cm
Inner annulus diameter	13.16 cm
Annular gap height	1.12 cm
Combustor length (from front end wall)	18.2 cm
H2 injection orifice diameter	1.19 mm
O2 injection orifice diameter	1.78 mm

2.2: SYSTEM CONTROL, DATA COLLECTION, AND PROCESSING

The control sequence and instrumentation are both controlled by National Instruments' LabView 2012 software. High speed pressure data is captured by a separate computer running LabView 2013 and a National Instruments DAQ.

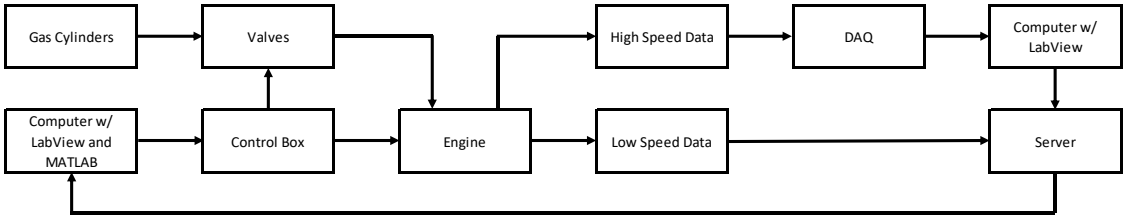

Figure 2.7. Block diagram of the system setup

After the two data files have been generated and saved on a server, they are run through a series of MATLAB programs that are designed to output useful plots for analysis. Detonation wave activity is observed by generating frequency response data using a fast Fourier transform of the high speed pressure data.

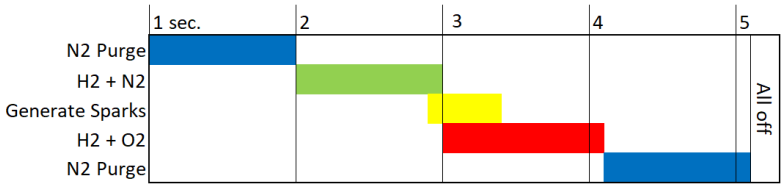

Figure 2.8. Current engine control sequence starting at t+1 seconds from user command.

Using a LabView Visual Interface (VI), a single command is sent to the control box which sets the system in motion. Following a 1 second delay, the sequence starts with an N2 purge through both oxidizer and fuel lines. At 2 seconds, H2 begins to flow through its line while N2 continues to flow through the O2 line. At 2.9 seconds, the spark control system initiates. H2+O2 begins at 3.0, and detonation typically occurs around 3.1 or 3.2 seconds. Fuel and oxidizer continue to flow after the sparking system has turned off and switches to N2 purge at 4.1 seconds. All valves are closed at 5.1 seconds.

2.3: TESTING PROCEDURE

The objectives of the aforementioned modifications were to prove or disprove the existence of supersonic flow from the engine, show the linkage of oblique shock waves to the normal detonation waves in the annulus, observe the effect on engine combustor pressure from varied downstream conditions, and use pitot tube and static pressure probe data to measure exhaust velocity.

Table 2.3. Engine operation parameters

Mass flow	~50 g/s total H2+O2
Equivalence ratio	1.0-1.1
Wave number	2
Butterfly valve settings	4.5, 5.0, 5.5, 6.0 psi

While the UW RDE system setup is designed to allow manual setting of fuel and oxidizer flow rates, a single operating point was used for all tests. Regulators were adjusted to deliver a total flow rate of about 50 grams per second at an equivalence ratio of nearly unity. This mass flow rate corresponds with 2 concurrent detonation waves. Four separate engine fires were conducted while adjusting the downstream butterfly valve to different settings, thus varying the back pressure within the sealed system.

2.4: EXPERIMENTAL OBJECTIVES

A brief summary of the objectives of this experimental process are as follows:

- Establish a link between the cold-side oblique shock wave being shedded by the normal detonation wave as it travels around the annulus

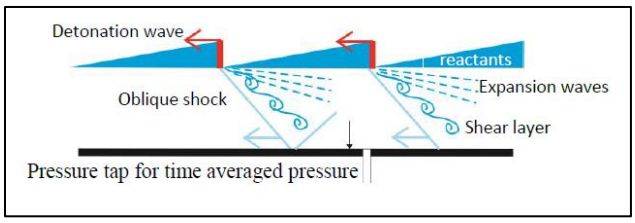

Figure 2.9. Diagram of cold-side oblique shock pattern linked to the normal detonation waves

- Prove or disprove the existence of throatless supersonic exhaust velocity by monitoring combustor pressures while varying downstream conditions.
- Directly measure combustor and exhaust Mach numbers to provide raw data of subsonic of supersonic flows from the engine.

CHAPTER 3: RESULTS AND DISCUSSION

3.1: A BRIEF EXPLANATION OF THE FOURIER TRANSFORM

A powerful tool used in data analysis is the Fourier transform, which is helpful in showing frequency patterns from a time signal. The Fast Fourier Transform (FFT) function is readily available in many software packages, including MATLAB, which will be heavily used for data analysis in this paper.

One of the peculiar characteristics of the Fourier transform is the appearance of harmonic frequencies. These harmonics are integer multiples of the original frequency response and they are the result of the Fourier transform and how it approximates the time signal as a sum of sine and cosine functions. Each of these individual sine and cosine functions have a unique frequency that correspond to the harmonic frequencies of the original response signal.

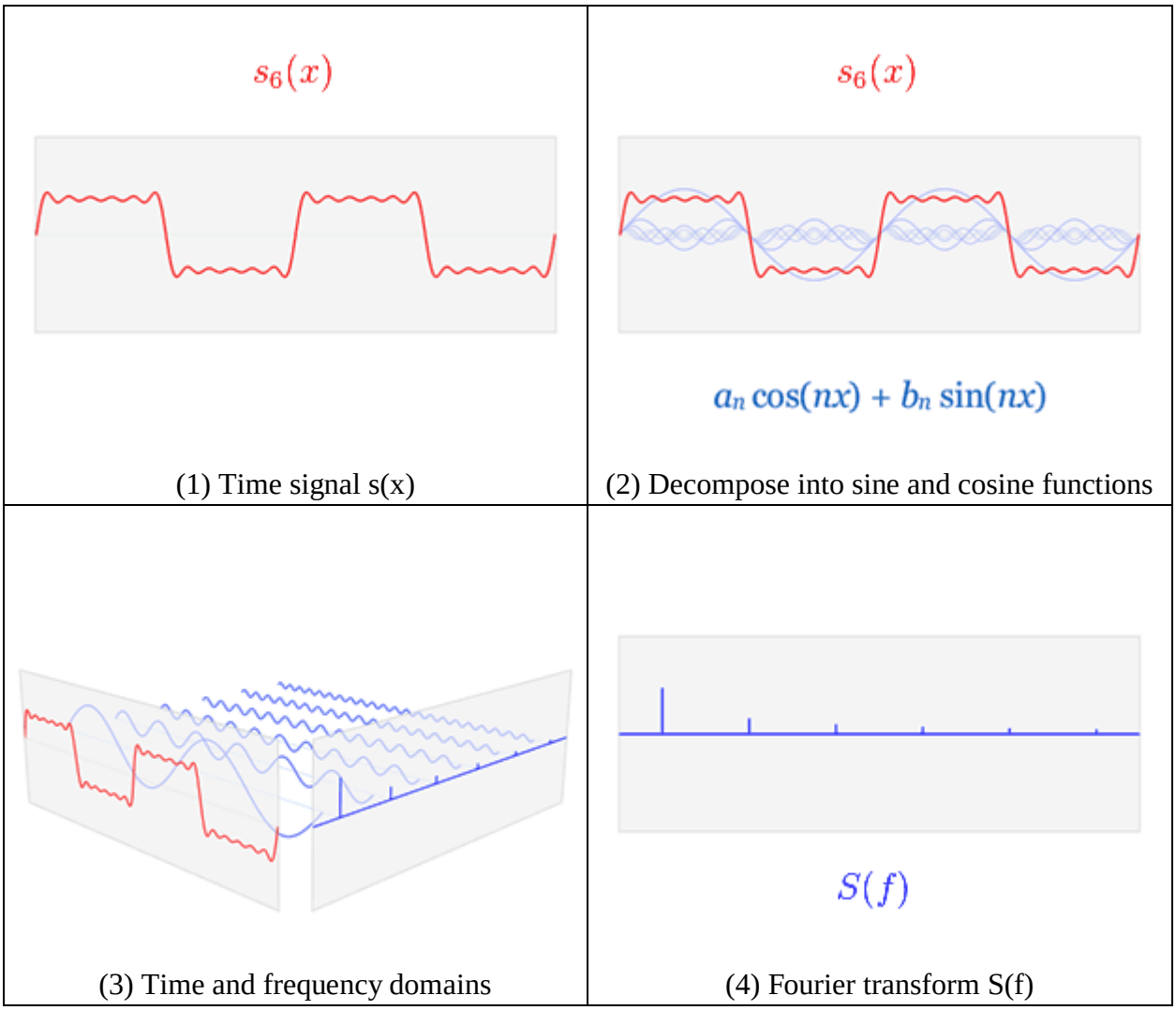

(1) Time signal s(x)

(2) Decompose into sine and cosine functions

(3) Time and frequency domains

(4) Fourier transform S(f)

Figure 3.1. Deconstruction of a time signal into the Fourier domain[ii]

3.2: RELATIONSHIP BETWEEN THE NORMAL DETONATION WAVEFRONT AND ATTACHED OBLIQUE SHOCKS

The most obvious and immediate experimental result was the linkage between the normal detonation wave and the oblique shock waves upstream. To reiterate, one high speed transducer was located on the engine side wall, approximately 1.5 inches downstream from the other sensor on the engine front endwall.

Typically, the fundamental frequency, f, of the detonation waves for this engine is observed to be about 4.25 kHz. This corresponds to one detonation wave within the engine.

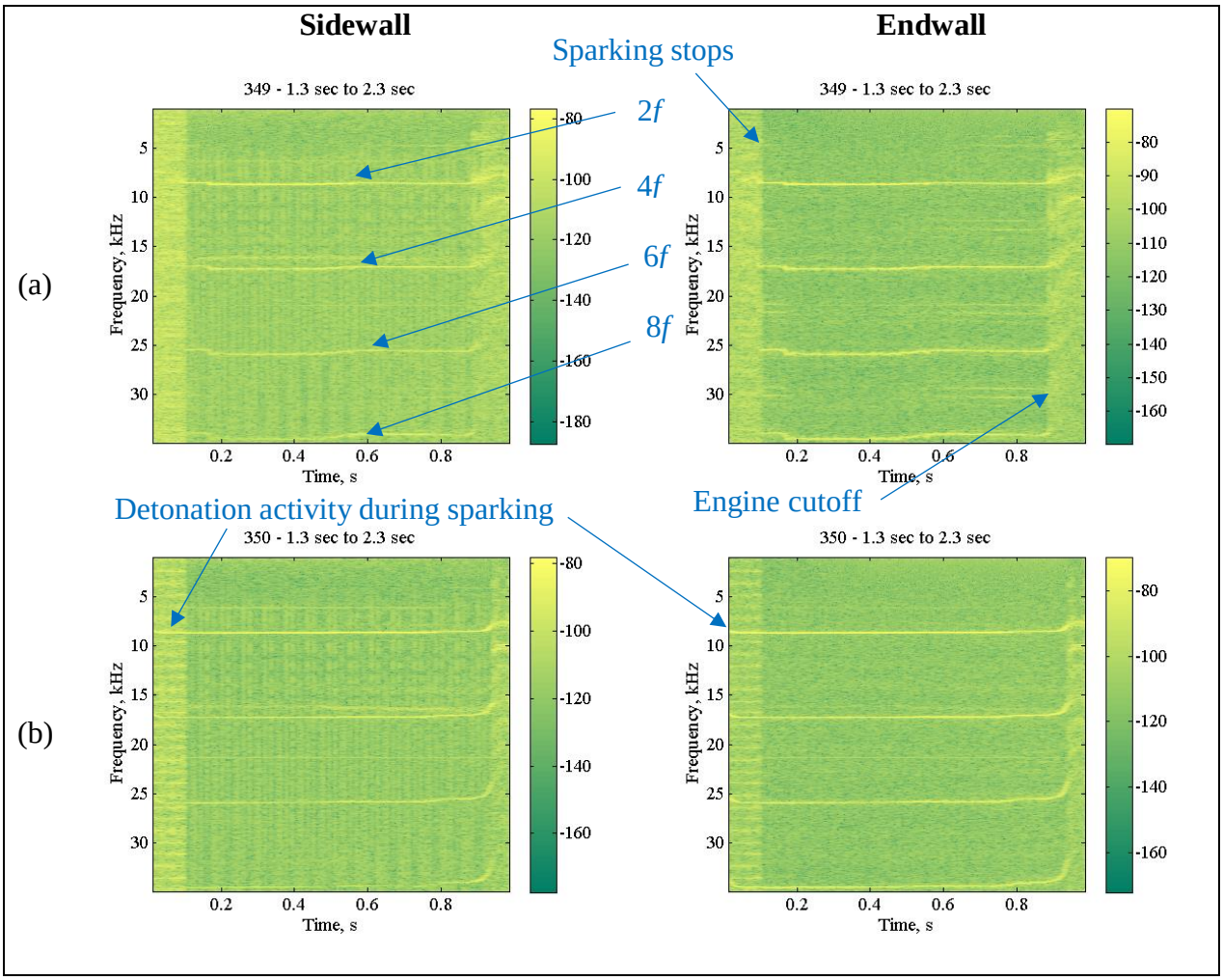

Figure 3.2. Frequency response spectrograms during engine operation with butterfly valve at (a) 5.5 and (b) 6.0.

There is a clear connection between the front endwall and sidewall pressure traces. This link is provided by the oblique shocks locked to the spinning detonation waves described in Figure 2.9. In the cases shown in Figure 3.2, the frequency, $2f$, was approximately 8.5 kHz, indicating that there were two concurrent detonation waves in the annulus for this engine setup[5]. Harmonic frequencies are also shown by the Fourier transform at $4f$, $6f$, and $8f$.

These plots simply look at the ~1 second of engine operation. The yellow-ish band on the left is the last 0.1 seconds of sparking. In some cases, detonation can be still be observed through the

noise generated by the sparking system, as shown in Figure 3.2b. Fuel and oxidizer valve cutoff time coincides with the 0.8 second timestamp on the above spectrograms. Detonation continues until fuel and oxidizer finally depletes from the manifolds upstream of the injection orifices.

3.3: EFFECT OF DOWNSTREAM CONDITIONS ON COMBUSTOR PRESSURES

Studying any change in combustor pressures as a result of altering the back pressure should qualitatively describe the exhaust characteristics of the RDE. To validate the effect of varying the butterfly valve position, the engine firing sequence was run, but only with nitrogen gas shown in Figure 3.3. These measurements were made by the time-averaged pressure sensor on the front end wall. As expected, the combustor pressures rose as the valve was turned to a more closed position. Some delay in the pressure drop off was also observed due to the more constricted flow into the dump tank. To clarify, the higher the pressure setting on the BFV, the more open it is to the flow.

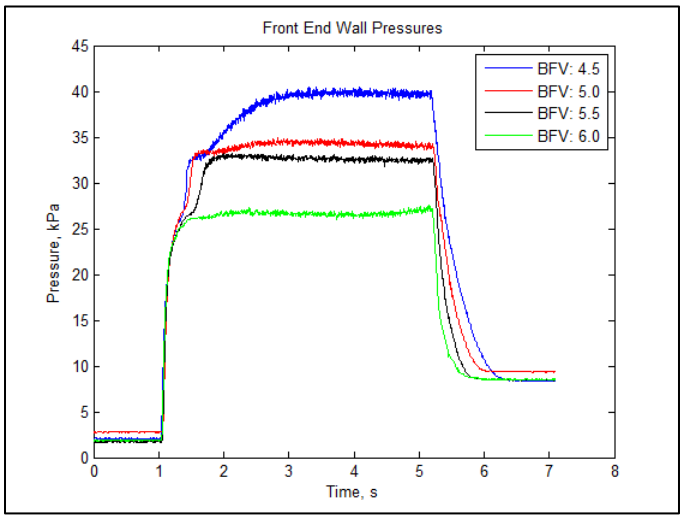

Figure 3.3. Combustor end-wall pressures during cold-shot tests

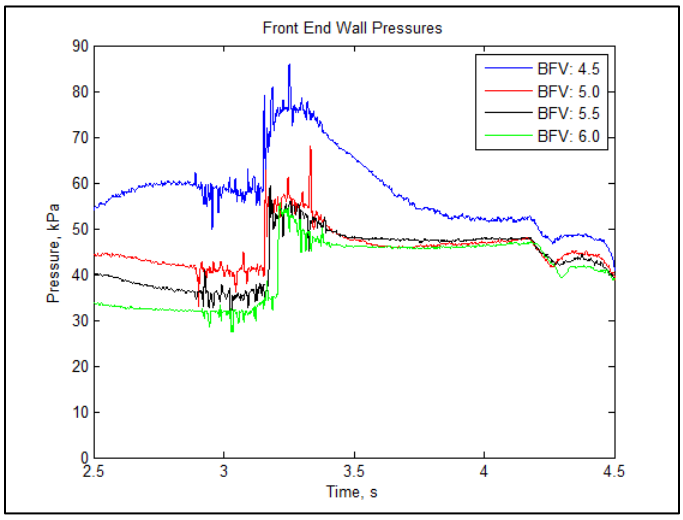

Figure 3.4 Combustor end wall pressures for all BFV settings during engine hot-fire

The hot fire tests in Figure 3.4 showed interesting trends. While the combustor pressures at the butterfly valve setting of 4.5 showed significant increase, the other three settings had negligible differences from each other. For these three examples, pre-ignition pressures where nitrogen purge was occurring had some deviation.

However, all pressure traces settled onto almost the same waveform after engine detonation had begun. This result suggests that the flow is, in fact, supersonic, as no downstream perturbations are allowed to travel back upstream to affect the combustor conditions.

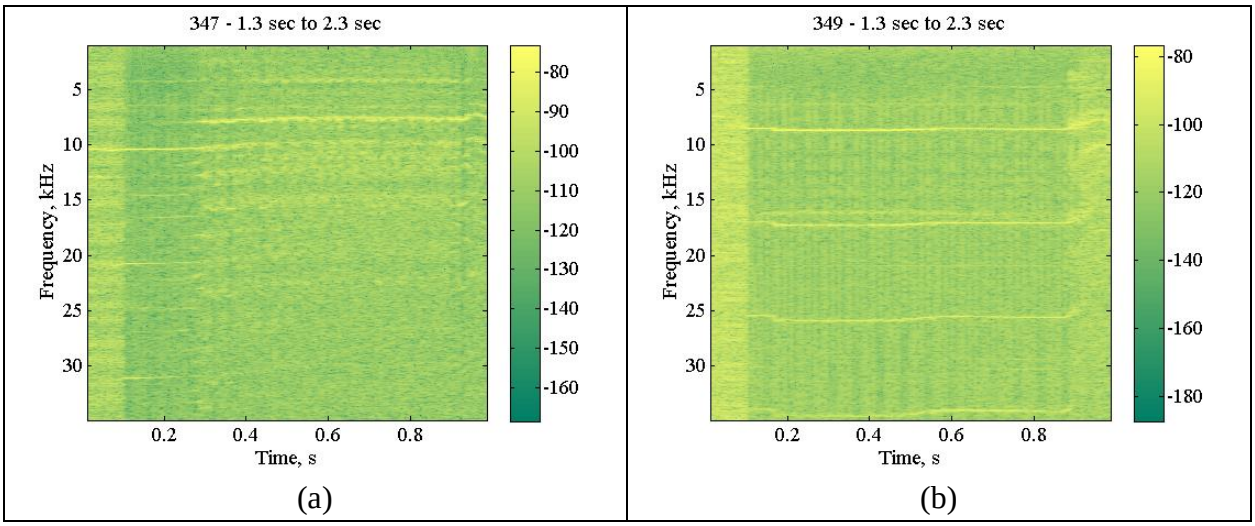

Figure 3.5. Spectrogram of hot fire runs with BFV set at (a) 4.5 and (b) 5.5

There appears to be a cutoff point where the "openness" of the butterfly valve meets the requirements for the mass flow leaving the engine. This may, in fact, cause the engine to "choke", as the spectrogram in Figure 3.5a for this test fire showed none or disorderly detonation behavior.

An additional test run at this BFV setting confirmed this non-operational condition. Since no orderly detonation occurred, the exhaust was not supersonic and the end wall pressure was allowed to stay built up. Spectrograms for the BFV @ 5.0 and 6.0 cases can be found in the Appendix section.

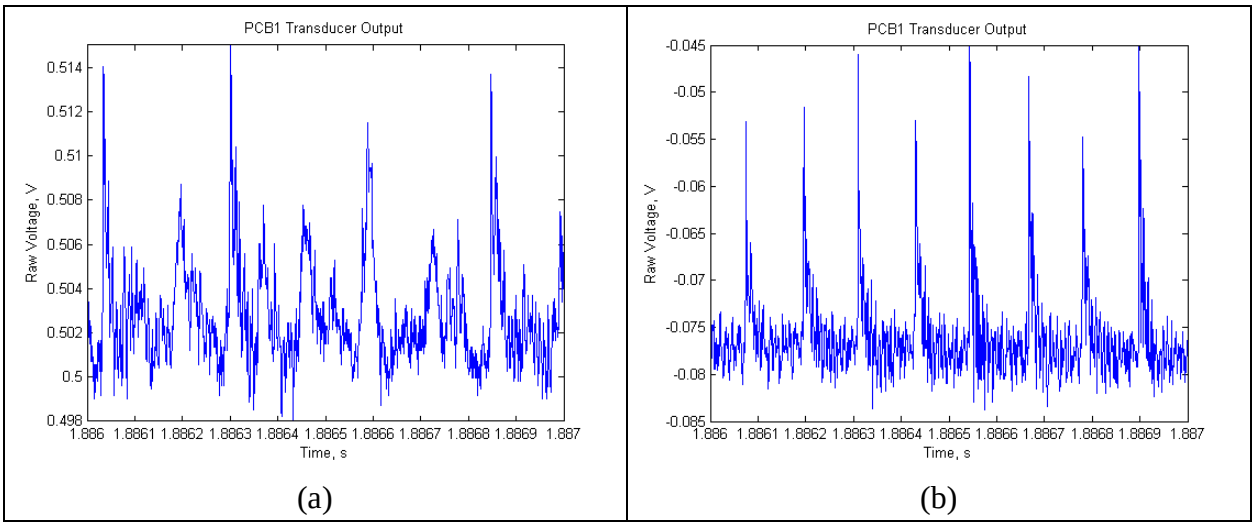

Figure 3.6. High-speed pressure transducer raw voltage for BFV set at (a) 4.5 and (b) 5.5

The appearance of some activity at about 10.5 kHz on the left side of Figure 3.5a is a common occurrence when detonation is not achieved during a hot fire. This same frequency is observed to be dominant when striking the test rig with a hammer and analyzing the air-borne frequency spectra. This image can be found in the appendix as Figure A.4. It could be that this is a natural frequency of the RDE in its current configuration. Additional investigation can be done to discover the true nature of this phenomenon.

While the front end wall pressure sensor data shows strong evidence supporting supersonic exhaust velocity, it must also be stated that this location is protected by the detonation waves sweeping by. This may actually grant immunity to interference from downstream perturbations. The Combustor 1 sensor is also upstream of the detonation zone and shows essentially the same

non-variance of pressures during proper engine operation. A look at the Combustor 2 sensor shows a slight variance, possibly spiking the supposition inferred by the other two sensors.

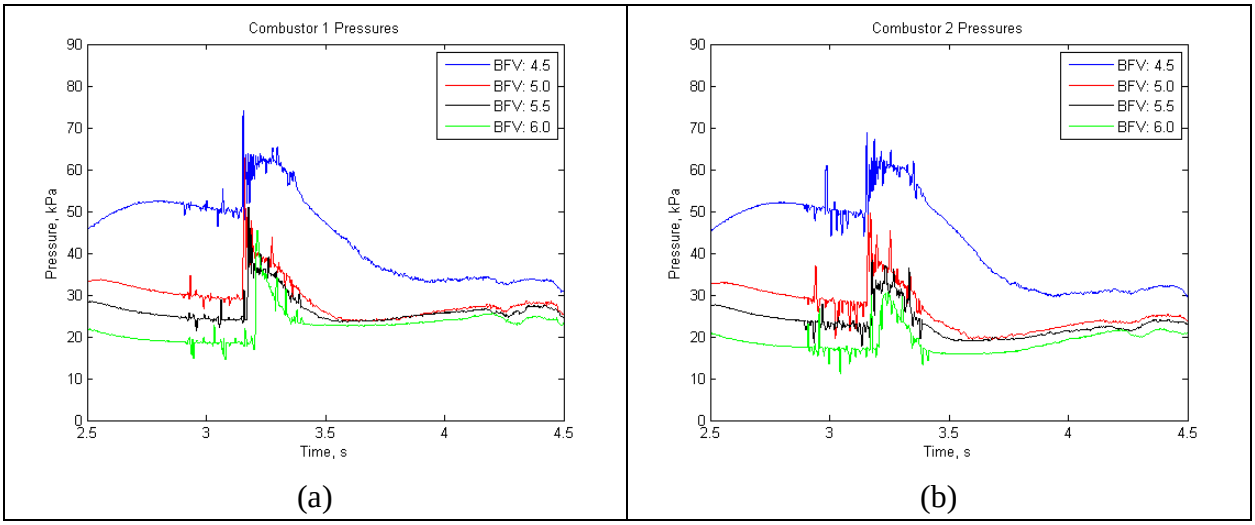

Figure 3.7. Combustor 1 and 2 sensor data during engine operation

The Combustor 2 sensor data shows a small amount of variance for each BFV setting. What must be considered, however, is the fact that the flows in this region are nearing or surpassing sonic absolute velocities. As shown later in Figure 3.11, the Mach number near this transducer increases for each case leading up to the BFV setting of 6.0. If this is because velocity is higher at this setting, then the static pressure will most likely be lower.

An astute observer would also notice that the combustor pressures for the hot fire tests have a higher initial pressure before the H2-O2 injection begins at the 3 second mark. During the cold flow tests, only N2 gas was used in both injector sets. For hot fire tests, H2 and N2 was injected into the combustor from 2.0 to 3.0 seconds, which would account for the discrepancy in pressures. Also, the noise present in the 2.9 to 3.4 second interval directly corresponds to the sparking time.

3.4: FRONT END WALL PRESSURE MEASUREMENTS

Observations made on the behavior of the front end wall time-averaged pressure transducer have raised some questions as to the validity of the magnitude of pressures seen in this region.

Qualitatively, the results discussed in the previous section are hard to dispute. But, the actual values are difficult to explain. Since the pitot tube should be aligned into the flow, albeit pointed downstream in the direction of expected flow, there is the possibility that these elevated pressures are reflective of the total pressure in the mixing area. By contrast, the combustor pressure transducers should be reading static pressures in the combustor. However, there should not be much axial velocity in this region upstream of the detonation zone, aside from momentum imparted on the fluid from the oblique shockwaves sweeping by. This would make sense, if not for the fact that the elevated pressure values shown in Figure 3.8a are also seen in the test runs using inert gases in Figure 3.8b. This behavior will be investigated and discussed in more detail in Part Two of this paper.

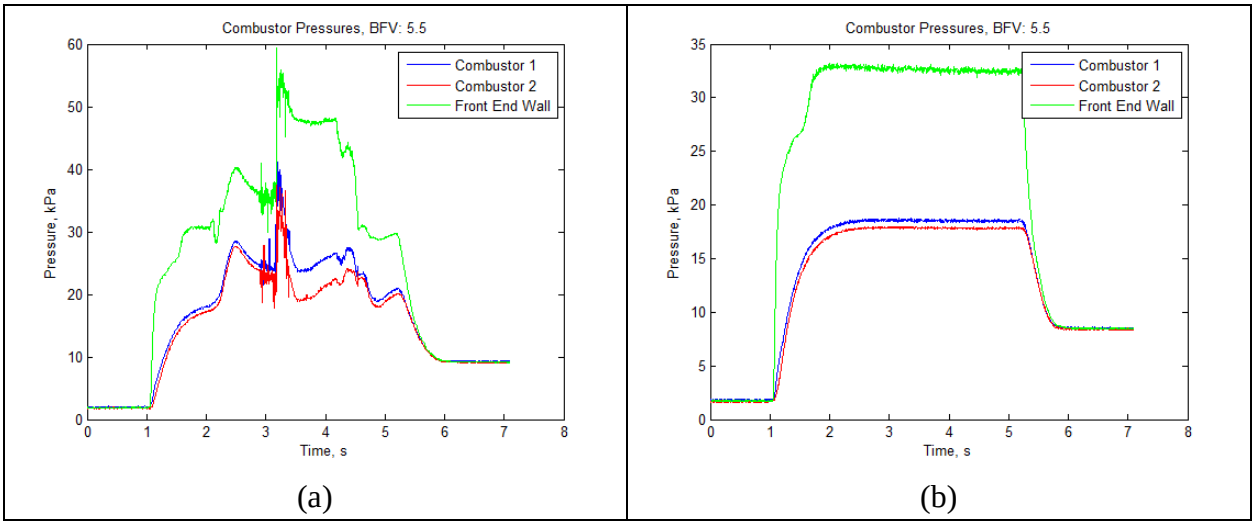

Figure 3.8. Combustor pressures for (a) hot fire and (b) cold fire tests

3.5: MEASUREMENT OF FLOW MACH NUMBER AND EFFECT OF EXPANSION NOZZLE

Working under the assumption that the exit velocity of the RDE was supersonic, attempts were made to quantify the Mach number at the combustor exit and measure the effect of an expansion nozzle attached to the end of the annulus.

In order to calculate the Mach number, the total pressure ratio formula was used:

$$\frac{P_0}{P} = \left(1 + \frac{\gamma - 1}{2} M^2\right)^{\frac{\gamma}{\gamma - 1}}$$

Supersonic velocities will require the Rayleigh pitot tube formula:

$$\frac{P_{02}}{P_1} = \left(\frac{(\gamma + 1)^2 M_1^2}{4\gamma M_1^2 - 2(\gamma - 1)}\right)^{\frac{\gamma}{\gamma - 1}} \cdot \frac{1 - \gamma + 2\gamma M_1^2}{\gamma + 1}$$

where P_1 must be measured in front of the bow shock created by the pitot tube in the flow.

The exhaust of the RDE is superheated steam, so a value of 1.2 for the specific heat ratio is assumed.

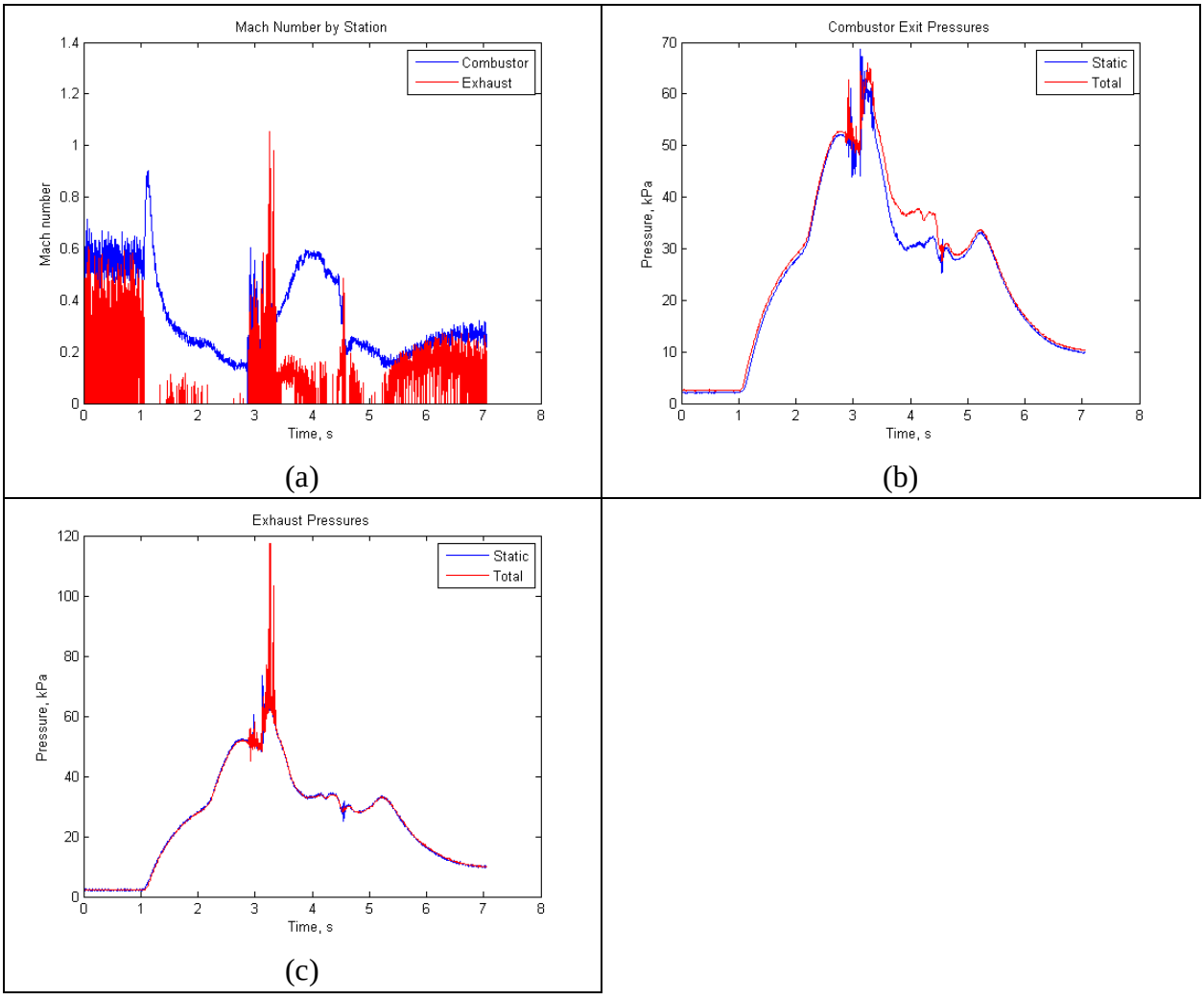

Figure 3.9. Flow Mach number, combustor pressures, and exhaust pressures for BFV setting of 4.5.

From the results in Figure 3.9, it is clear that there are issues in gathering total pressure data in the exhaust section. Several attempts were made to rectify this issue, but none yielded any improvement. Research done on this issue has been performed in the past and is described in detail in [4]. High-speed piezoelectronic sensors may yield more information, but the outlook is grim. The reason for this is that the exhaust gases are not flowing in a uniform direction; there is a general bulk flow, but local flows tend to exhibit "positive" and "negative" swirl. The direction of these local flows radially oscillate as the oblique shocks sweep by. Time-averaged sensors, such as the ones used during this experiment, are susceptible to this kind of flow behavior and are not to be trusted. Another measurement technique will probably have to be discovered to measure true axial exhaust velocity in the RDE.

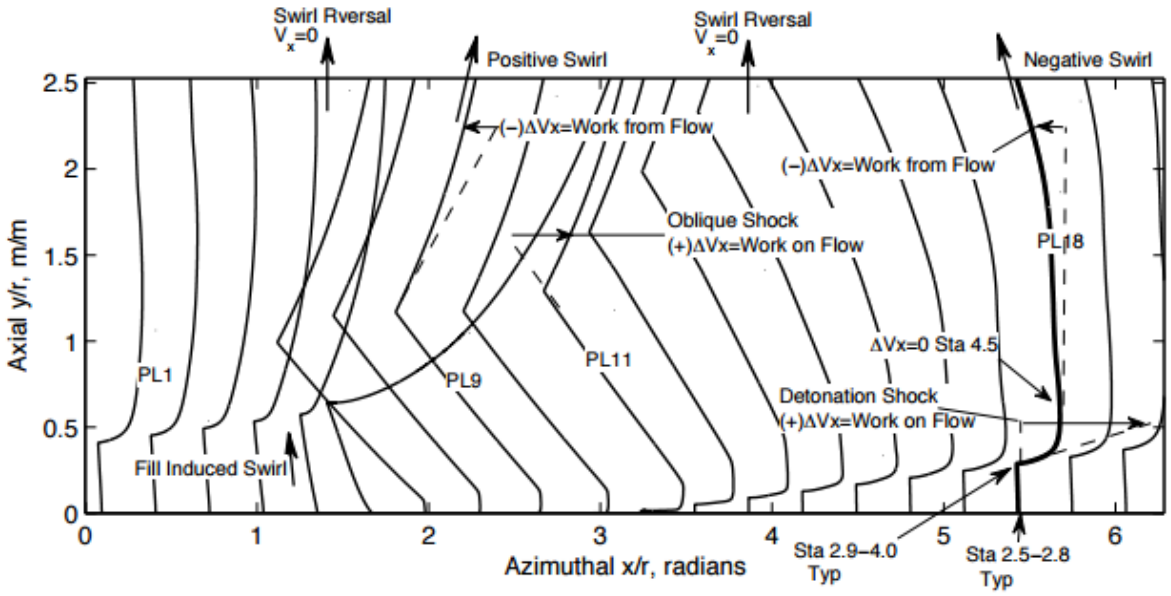

Figure 3.10. RDE flow time-averaged pathlines in the lab frame created by numerical simulation[4]

All combustor Mach number calculations are compiled into Figure 3.11 for brevity. This plot shows that there is a trend of increased exhaust velocities: the more open the butterfly valve, the higher the axial velocity.

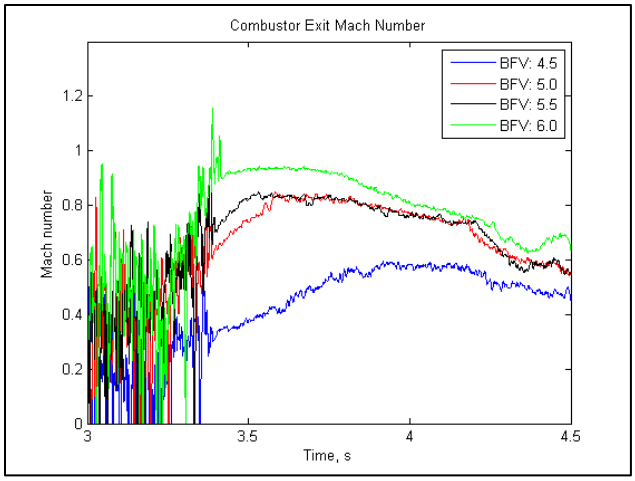

Figure 3.11. Composite plot of combustor exit Mach numbers

There is a degree of uncertainty in the pressures being read by the combustor pitot tube, however. Several influences must be taken into consideration. First, the pitot tube is constantly being buffeted by oblique shock waves from the normal detonation waves upstream. Second, the extreme temperatures of this region have an adverse effect on the structural integrity of the tube, as shown in Figure 3.12. Effects of extreme heating could have caused some warping. Finally, the degree to which the tube was accurately aligned into the flow is suspect. Markings were made on the standoff tubing leading to the transducer, but it was difficult to make sure it was exactly lined up. Also, each successive test fire could have displaced the tube's alignment with respect to the flow a little at a time. Upon removing the tube after the four test firings, it was difficult to tell if the tube was correctly oriented.

The results seen from the combustor exit sensors seems to be in direct contradiction with the issues facing the measurement of the exhaust velocity past the expansion nozzle, however. Why is it that total pressure can be picked up in the combustor, albeit with some questionable accuracy described above, but not in the exhaust expansion section? Additional work and/or research will have to be done to find a possible answer.

Figure 3.12. Partially melted pitot tube used in the combustor region.

The flow velocities seen within the combustor are promising and agree with the results of the effects of back pressure on the engine conditions. With lower back pressure, the exhaust accelerates to near sonic speeds. High back pressure appears to have an averse affect on engine operation, and it is also believed that, conversely, opening the BFV too wide will prevent proper engine operation, as the fuel and oxidizer are blown downstream too quickly. Previous tests have confirmed this behavior, but the results discussed in this section lend to a sense of curiosity as to whether the combustor flow can actually reach sonic and supersonic velocities before this operation threshold is reached.

CHAPTER 4: CONCLUSIONS AND RECOMMENDATIONS

Through experimental testing and data analysis, the objectives outlined were either confirmed, denied, or given additional credence to their validity:

- The existence of oblique shocks sweeping through the cold mixing area upstream of the detonation zone was confirmed by Fourier transform of high-speed pressure sensor data.
- This mixing area was also shown to be immune to downstream effects, most likely due to the extreme velocity and frequency of the detonation waves sweeping by. Sensor data downstream of the detonation zone also showed very little reaction to these changed conditions, although what variations in pressure existed could easily be explained away by the presence of increased flow velocities which drive down the static pressure as a result.
- Measurement of exhaust Mach numbers was shown to be impossible, validating previous work done using numerical simulations and laboratory work on this subject.

To be clear, these results do not prove the existence of supersonic flows; they merely offer strong supporting evidence to the affirmative. A brief summary of future work includes:

- Discover a method to accurately measure the velocity and/or Mach number of the exhaust bulk flow.
- Explore the effect of increasing mass flow on the measured combustor Mach number
- Determine what, if any, minimum back pressure is required for consistent RDE operation by continuing to open the butterfly valve even more. At the same time, continue to monitor combustor Mach numbers to see if they increase beyond a measured Mach number of unity. Of course, the application of the Rayleigh pitot tube formula is strongly suggested.

To facilitate future work, a few suggestions for test rig modifications are as follows:

- A force-balance or thrust gauge would be helpful to provide additional data during future experimentation.
- Replace constricting ducts downstream with constant-area geometry. Some of the ducts downstream are not the same 6" ID as the engine's outer annulus.
- Add additional instrumentation ports in the engine exhaust section. Considerations can also be made to accommodate some kind of visualization scheme to see inside during operation.
- Install a series of ports for high-speed piezoelectric pressure transducers axially along the combustor in an attempt to determine the axial location of the detonation zone.

Part Two
Numerical Analysis of Mixing in the Combustor

CHAPTER 5: CONSTRUCTING THE MODEL DOMAIN

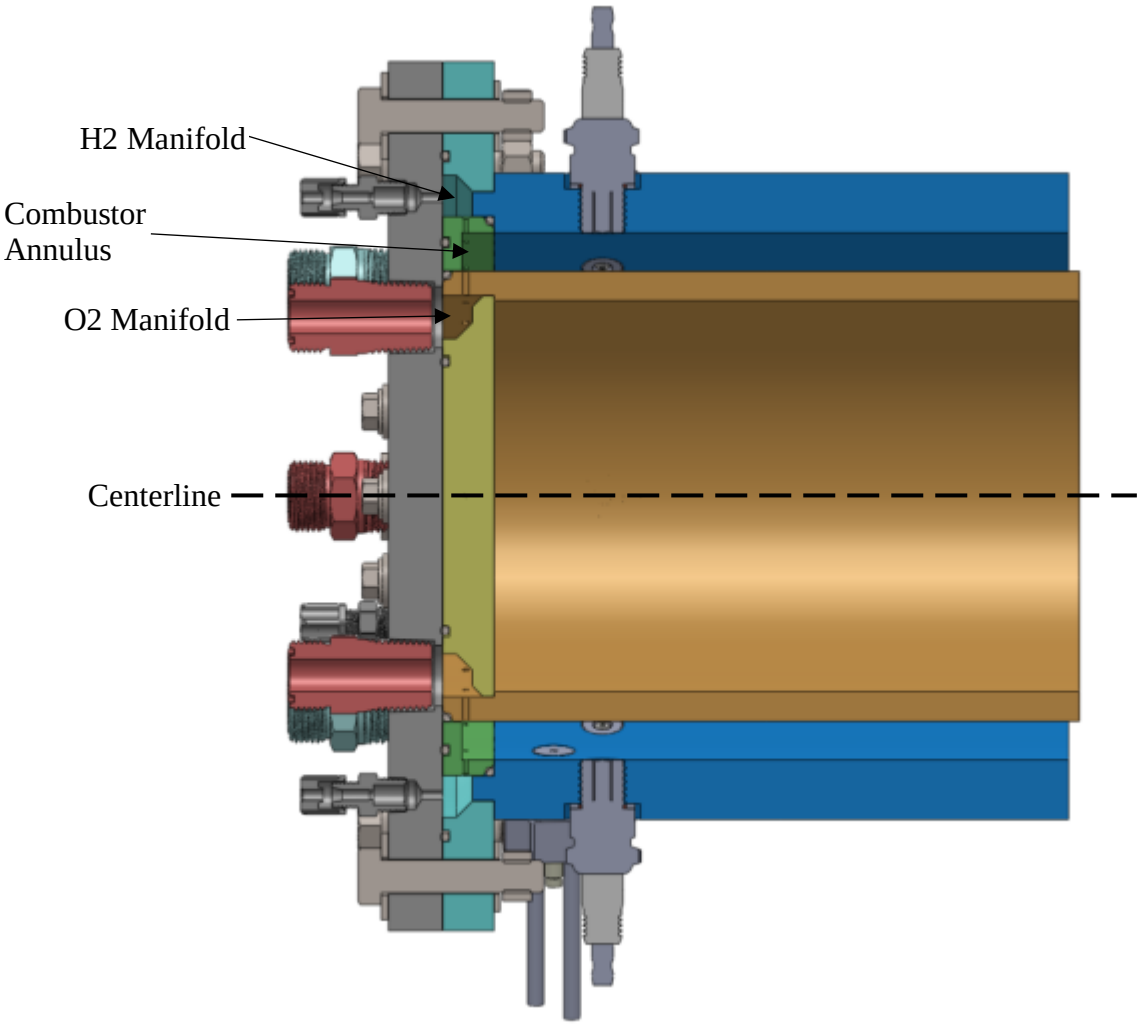

Figure 5.1. Solidworks model cutaway of the UW RDE[1]

The internal geometry of the RDE consists mainly of the H2 manifold, O2 manifold, combustor, and both sets of injector orifices. There are 24 fuel and oxidizer orifices each, for a total of 48. As

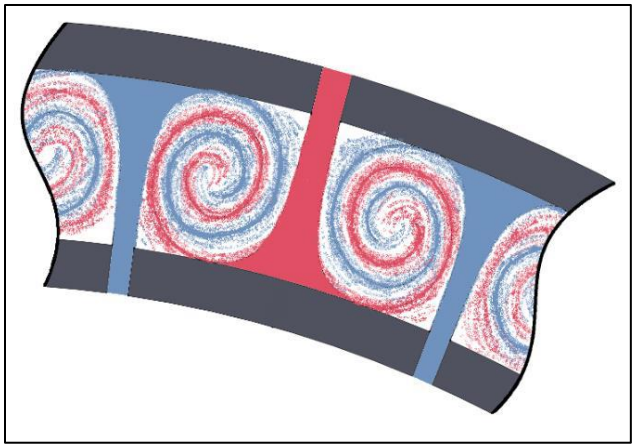

Figure 5.2 Sketch of vortical entrainment due to staggered injector orifices[1]

mentioned at the beginning of this paper, these tiny ducts are arranged in a staggered pattern so that the jets impinge on the opposing wall inside of the combustor annulus. The objective of this injector arrangement is to encourage high mixing efficiency by vortical entrainment of the flows. If this phenomenon is indeed present, it should reduce the axial length required before the fuel and oxidizer reach a level of sufficient "detonability".

The internal volume was extracted from the SolidWorks model of the RDE using the SpaceClaim geometry editor that comes with Ansys Fluent 17.2. Some of the geometry was simplified to help expedite the solution convergence. This includes slicing the model into a 1/8 radial symmetry section. The combustor duct was also shortened since it will not yield much useful downstream information anyways. The injector orifices from each manifold are not equal in diameter; refer to Table 2.2 for dimensions.

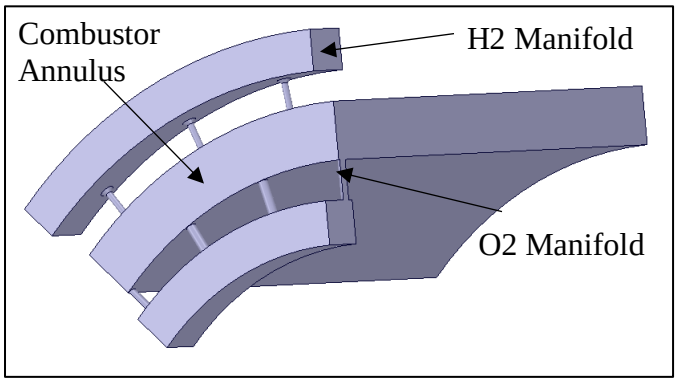

Figure 5.3. Volume extracted from one-eighth section of the RDE. The combustor has also been truncated.

CHAPTER 6: SOLVER SETUP

An adapted mesh was used to increase resolution of the pressure gradients expected in the model. An initial number of iterations were calculated to generate preliminary contours, which served as a guide to further increase the mesh resolution. In this case, gradients of total pressure

were used as the criteria. Adaptation increased cell resolution from 123k count to 4065k count, the vast majority of which are concentrated in the injection area of the model.

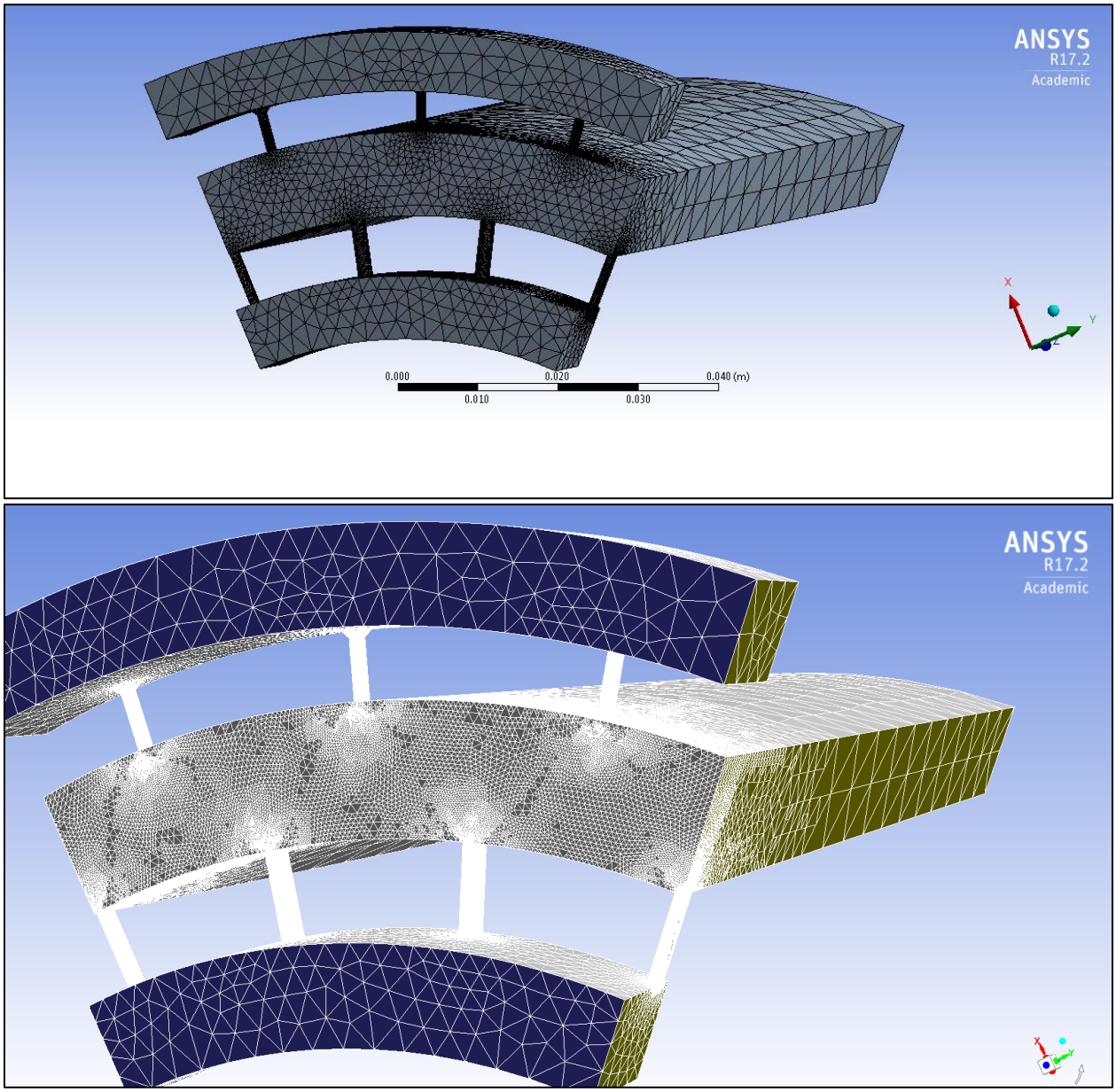

Figure 6.1. Standard mesh (above) compared to adapted mesh (below)

Boundary conditions were set using experimental data in order to simulate the flow behavior under a real-world condition. For simplicity, this model was run using only nitrogen gas through both inlet manifolds. Fortunately, such a test case already existed: the cold-shot data from Part One of this paper. However, it was proven through several tries in the fluid modeler that relying

on the Venturi flow meters for flow rates yielded unreasonably high manifold pressures. These flow rates are calculated using both compressible and incompressible forms, but were not used for the final model solution. Switching to the "manifold" flow calculation from the MATLAB output produced a more accurate solution. The manifold flow rate calculation is based on the flow through a choked orifice,

$$\dot{m} = C_D A \sqrt{\gamma \rho_0 P_0 \left(\frac{2}{\gamma+1}\right)^{\frac{\gamma+1}{\gamma-1}}}$$

$$= C_D A \sqrt{\gamma \frac{P_0^2}{RT_0} \left(\frac{2}{\gamma+1}\right)^{\frac{\gamma+1}{\gamma-1}}}$$

The discharge coefficient used was 0.7 and 0.9 for the O2 inlet and H2 inlet, respectively. These values are based on the geometry and Reynolds number and are essentially independent of the gas being used. Cross-sectional area is calculated from the orifice geometry described in Table 2.2. The flow conditions upstream of the orifice is nearly stagnant, so the manifold pressure data is used for total pressure. Since nitrogen is a diatomic gas, the specific heat ratio is a solid 1.4. Total temperature is assumed to be standard lab conditions, 300 Kelvins.

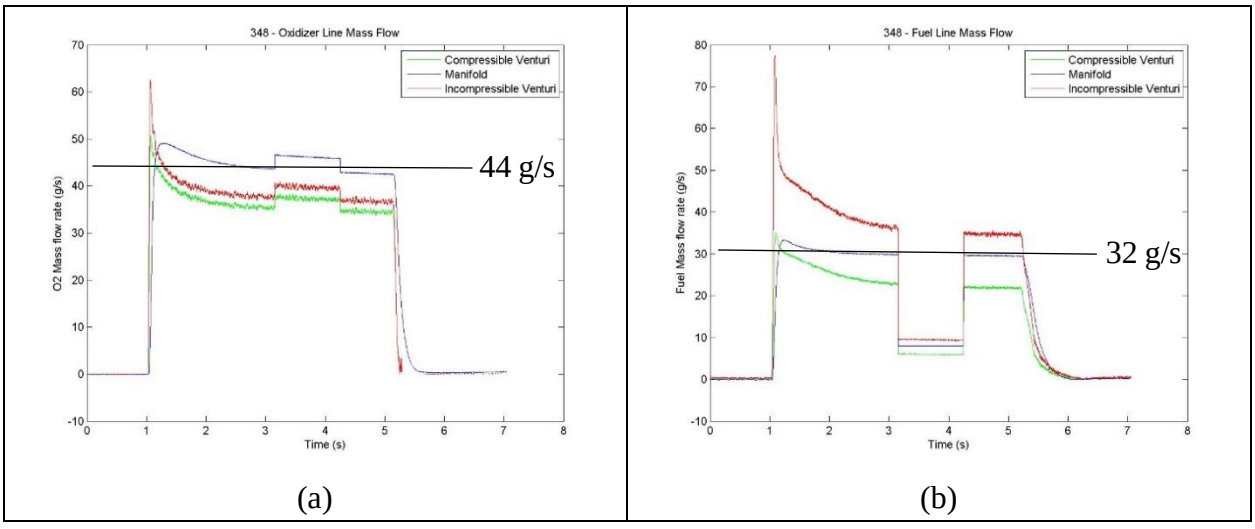

Figure 6.2. Experimental data used for model inputs of inlet mass flow rate

It should be noted that while running the cold shot experiments with nitrogen only, the LabView VI was not altered to change its mass flow calculation. This is why the values abruptly change during the 3-4 second window in Figure 6.2. The specific gas constant in the calculations is changed during this time interval to account for the change in gases from N2 to O2 and H2. For the purposes of this model, a steady-state value was used for flow rates: 44 g/s for the oxidizer manifold and 32 g/s for the fuel manifold. Since the geometry in the model is 1/8 symmetry, these values were divided by a factor of 8 when setting mass flow values in the boundary conditions.

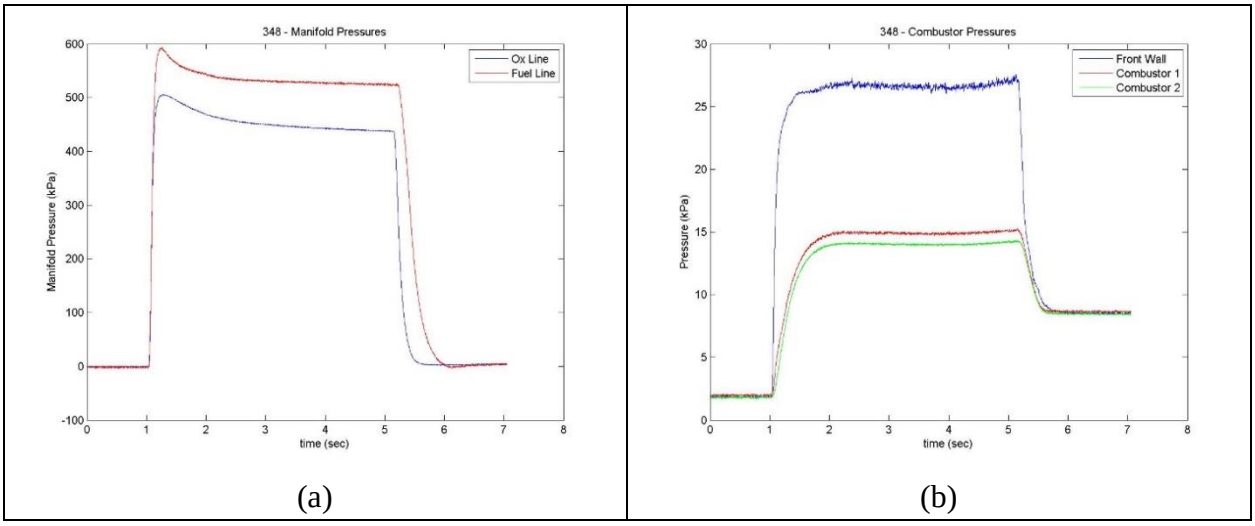

(a) (b)

Figure 6.3. Experimental data used for (a) initial guesses for inlet pressure and (b) combustor sensor validation

With the "Pressure Inlet" selection in Fluent, inlet total pressure is entered in the modeling setup conditions as an initial guess, along with the aforementioned mass flow. The pressure readings from the experiment serve as a good guess here, 550 kPa and 450 kPa for the fuel and oxidizer manifolds, respectively. Fluent will resolve the manifold pressures during convergence, based on the boundary conditions set before solving.

The sensor readings in the combustor, shown in Figure 6.3b, also factor in on setting up the initial conditions. The "Combustor 2" sensor corresponds to the exit on the physical engine and it is this reading that is used in the model for outlet conditions. The outlet type used in Fluent was

"Mass Flow Outlet", because this is the most desired selection for the expected model conditions. However, the pressure value entered here appears to be a constraint on the model and, if used, forces the solution to converge around the specified outlet condition. The other option is to target a set mass flow. With this option, the exit pressures will resolve around conserving mass flux. Unfortunately, attempts at using a target mass flow resulted in unreasonable manifold pressures and outlet pressures. For this model, outlet conditions were set at 13 kPa, as shown in the above figure.

Also, keep in mind the increased value of the "Front Wall" pressure sensor in Figure 6.3b. The validity of this transducer output was long in question after installation and part of the motivation for this fluid modeling was to either prove or invalidate the mysteriously high pressure values.

Since the flows are not expected to reach high Mach number, the default pressure-based solver was used and the Pressure-Velocity Coupling method selected was "Coupled" (default value is "SIMPLE"). The "Coupled" setting is best for compressible flows and is useful for this model since there will be some compression behavior in the manifolds and injector orifices. Courant number, or CFL, was dropped from the default value of 200 to 20 for the majority of iterations. Higher values (with an excellent model and initial conditions) will lead to faster convergence, but also have a greater chance of causing the solution to reach an undesirable divergent state if the non-optimal settings or complex geometry are used. Throughout the convergence process, it is good practice to watch the behavior of the residuals, adjusting settings as necessary. In this case, the CFL number was dropped when residuals leveled out.

Since there is significant compressible flow behavior, the density property of the N2 gas was set to "ideal-gas", which required the energy equation solver to be activated. To handle turbulence

modeling, the one-equation Spalart-Allmaras model was selected. All other settings were left at default values.

Convergence monitoring is a bit of art, rather than science. It is generally preached by the creators of Fluent that the residuals for all equations should drop three orders of magnitude before a solution can be considered "converged". However, input from experienced users indicates that this is not always the case. The model for this engine was showing difficulty reaching this requisite three orders of magnitude residuals reduction. Instead, the total mass flux through the engine was used as additional convergence criteria. A monitor was set up to keep track of this variable through each iteration.

CHAPTER 7: RESULTS AND DISCUSSION

7.1: RESIDUALS CONVERGENCE MANAGEMENT

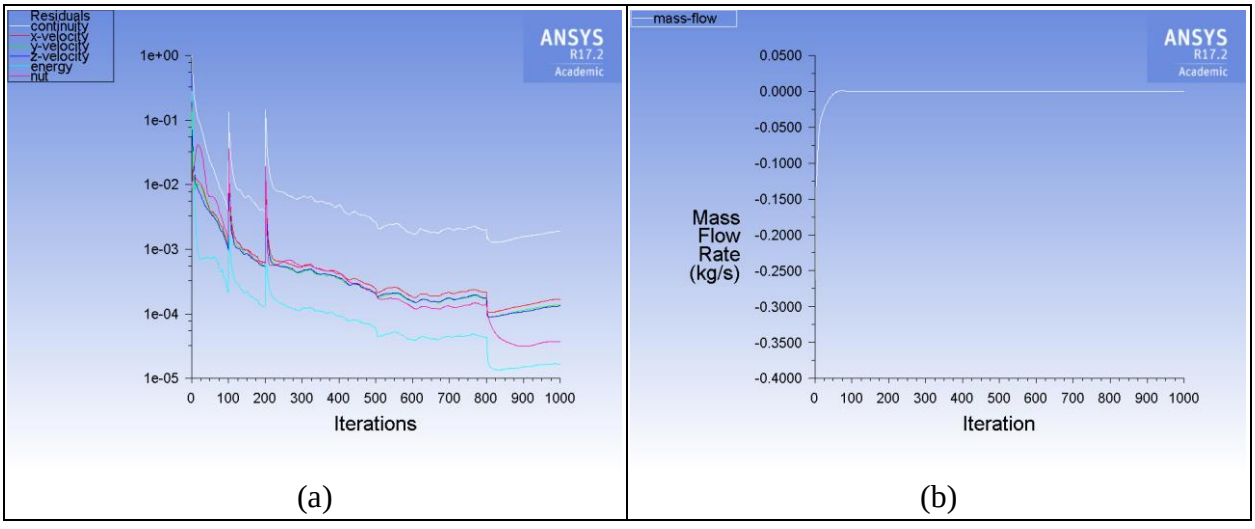

Figure 7.1. Residuals and convergence criteria used to establish model validity

Residuals, shown in Figure 7.1a, achieve some modicum of convergence, dropping nearly the requisite 3 orders of magnitude, as discussed earlier. The spikes correspond to mesh adaptation at both 100 and 200 iterations, followed by sudden drops due to lowering the CFL to help reduce

residuals even further. Figure 7.1b shows the very sudden convergence of mass flux through the system, and the steady state it maintains throughout the reiteration process. Using these criteria, it can be strongly argued that this model is adequately converged.

7.2: PRESSURE CONTOURS

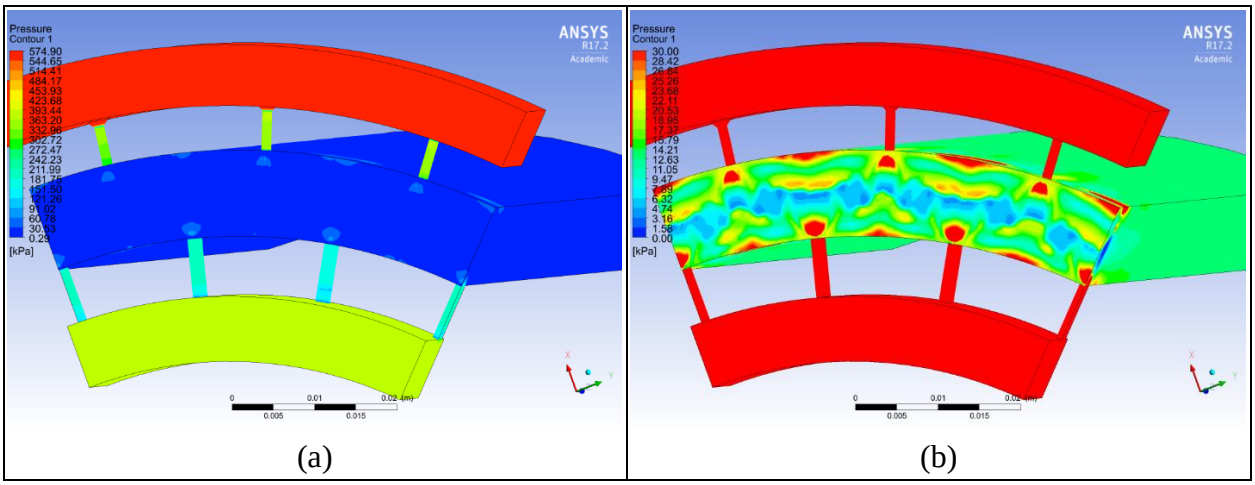

Figure 7.2. Pressure contours in the range of (a) 0 to 575 kPa and (b) 0 to 30 kPa

Figure 7.2a shows the magnitude of manifold pressures after reaching solution convergence. The pressures seen here are ~575 kPa and ~380 kPa for fuel and oxidizer manifolds, respectively. Referring back to Figure 6.3a, the expected manifold pressures are 550 kPa and 450 kPa. These model values appear to be within reasonable agreement.

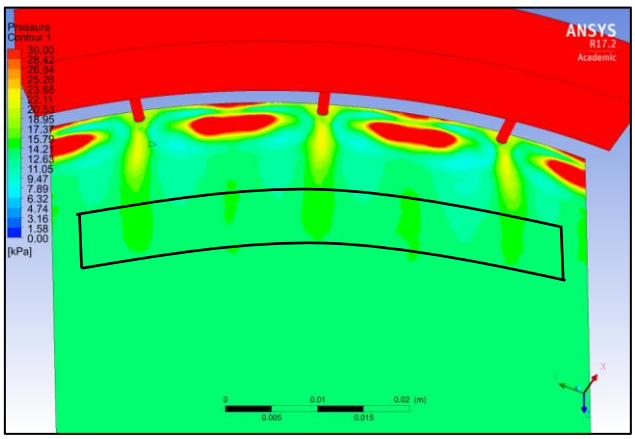

Figure 7.3. Engine sidewall pressure contour with possible sensor location outlined in black

The "Combustor 1" sensor is located a short distance downstream from the front end wall. However, the exact radial position of the sensor port in relation to the injector orifices is unclear at the time of the writing of this paper. Figure 7.3 illustrates the possible locations,

based on its axial position. Here, it can be seen that the pressures can vary from 14 to 16 kPa, which clearly agrees with the experimental sensor data in Figure 6.3b.

When plotting the pressure contour range of 0 to 30 kPa, as seen in Figure 7.2b, a peculiar region of higher pressure forms on the front wall, directly above the O2 inlet orifice. Using the Probe tool in CFD-Post shows the pressure in this region tops out at about 24 kPa. This value matches up well with the sensor reading in the aforementioned figure. What, then, is the nature of this mysterious high pressure bubble that is forming on the front end wall?

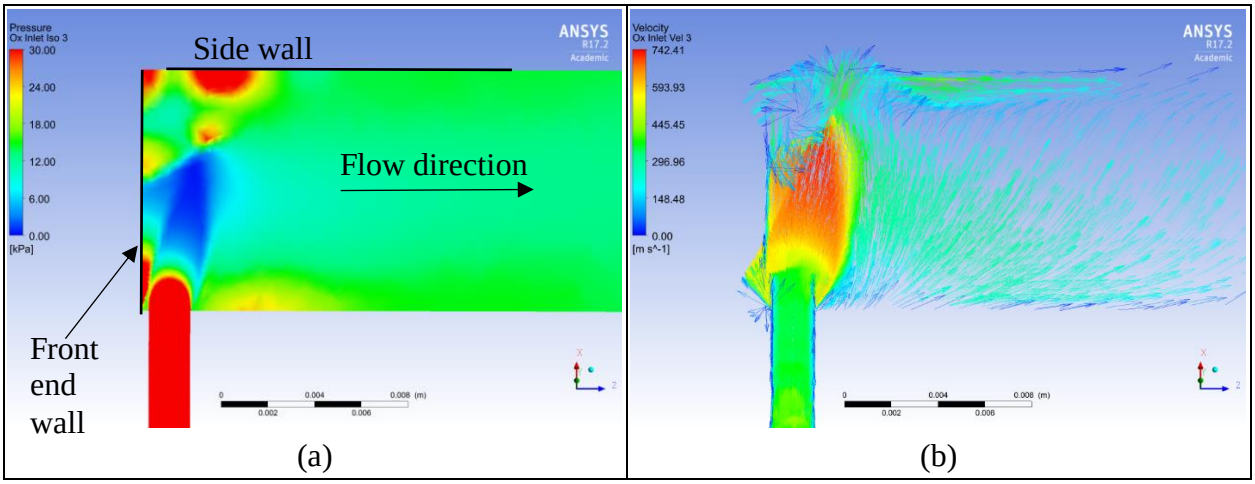

Figure 7.4. Side views of (a) pressure contour and (b) velocity vectors on a plane bisecting an O2 injector orifice

The answer can be seen in Figure 7.4b, where a recirculation zone has appeared in the corner opposite of the injector orifice. The local velocity of this flow is significantly reduced from the high values seen in the jet plume, causing static pressure to rise. The pressure sensor in question is located approximately midway along the front end wall. While the high pressure zone doesn't quite reach all the way down to the halfway point in this model solution, it is entirely within the realm of possibility that this recirculation zone has a slightly different behavior and/or shape in real life. Qualitatively, this model offers a strong explanation as to the true nature of the high pressures seen in the front end wall sensor when compared to the sidewall sensors. If, for example,

the inlet velocity was different than seen in the model, the recirculation zone could be even bigger

33

than shown here. Also, the supersonic plume will likely form a Mach disc at some location above the injector orifice. It appears that this model does not accommodate this phenomenon with the current settings. However, this Mach disc will also have a major effect on flow conditions near the front end wall in reality.

7.3: VORTICAL ENTRAINMENT OF FLUIDS

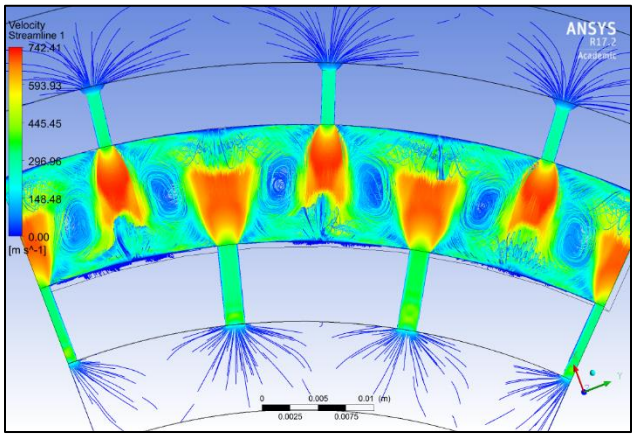

Figure 7.5. Front view of 3D streamline plot

The characteristics of the flow can be illustrated with amazing fidelity by using a streamline plot within CFD-Post. An isosurface was created in the post-processing program bisecting all injectors latitudinally, which was the basis for the seed points that generated these streamlines. Vortical entrainment of the individual flows is obvious at a glance in Figure 7.5, along with the presence of the recirculation zones along the walls opposing each injector orifice. Also, given that the ambient pressure is approximately 13 kPa, the fluid jets exhibit large plumes in the combustor section, much like a rocket exhaust. This streamline pattern looks awfully familiar…

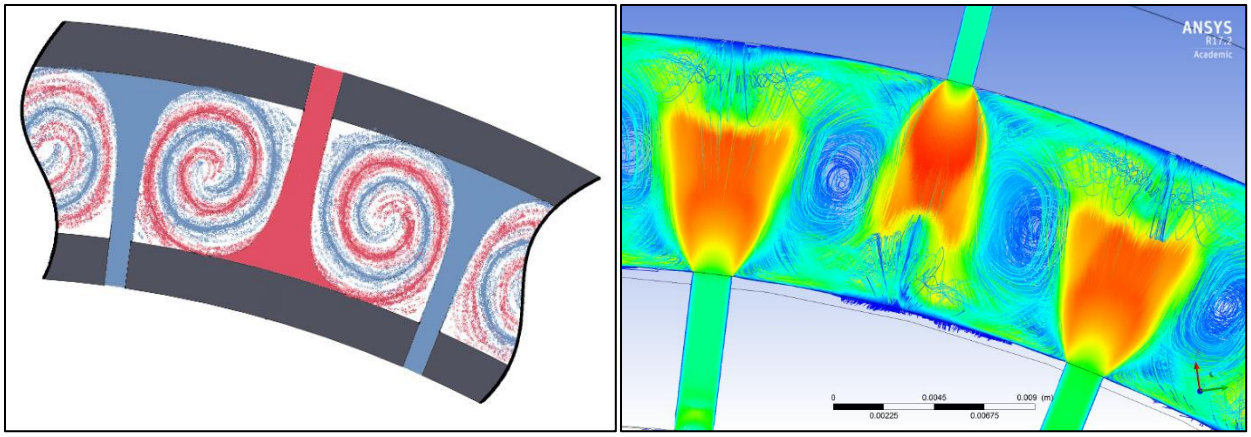

Figure 7.6. Comparison of predicted vortical entrainment with CFD model results

As seen in Figure 7.6, the initial sketch was not far off. Given, that the CFD model is showing three-dimensional behavior, it's easy to see that the same, or similar, results could be seen on a 2-D plane of streamlines. However, there exists some technical difficulty in generating such an image with this software. This will be left to the reader's imagination.

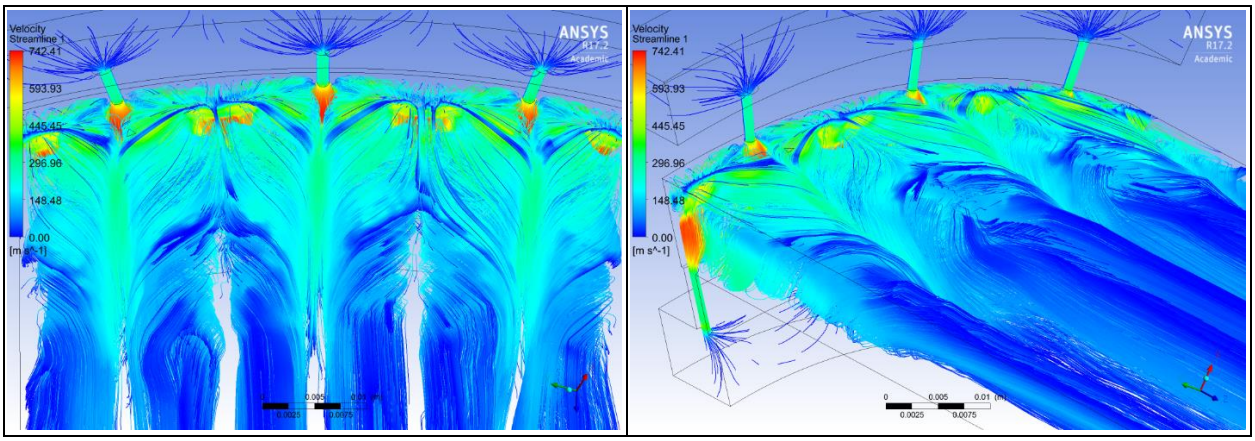

Figure 7.7. Sidewall and isometric views of 3D streamline plot

The streamline plot was extremely revealing in regards to the flow visualization during injection. In Figure 7.7, counter-rotating vortices persist downstream for some time, continuing to encourage fast mixing. These vortices appear to stay within their respective confined regions even far downstream. Of course, this is not illustrative of the flow behavior during a real engine hot-fire.

7.4: EFFECT OF JET IMPINGEMENT ON COMBUSTOR WALLS

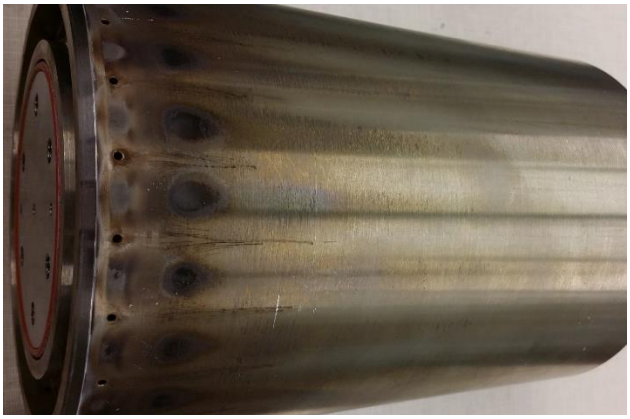

Figure 7.8. Combustor inner annulus wall after almost 100 engine hot-fires[1]

An astute observation has been made using these streamlines. The patterns shown correspond somewhat to discoloration markings seen on the combustor walls after engine disassembly. However, the vortex "cells" in the CFD model are too narrow in width to offer reasonable explanation. The dark markings shown in Figure 7.8 are radially aligned with the H2 injectors, as the orifices seen on the left side of the figure are O2 injectors. These dark markings could possibly be the result of molecular diffusion from the jet impingement from the fuel injector. However, these marks are much further downstream than what would correspond to the impingement area in the CFD model. There is a strong possibility that the aforementioned recirculation zone is even greater in magnitude in reality. This large pressure gradient would cause the jet to cant even futher downstream. The high-velocity gases collide with the high temperature stainless steel wall during and after engine operation. These conditions could lead to some diffusion effect, the process of which is repeated with each engine firing. It is highly likely that this is a nitriding of the steel surface, due to the nitrogen gas impinging onto the hot inner annulus after a hot fire.

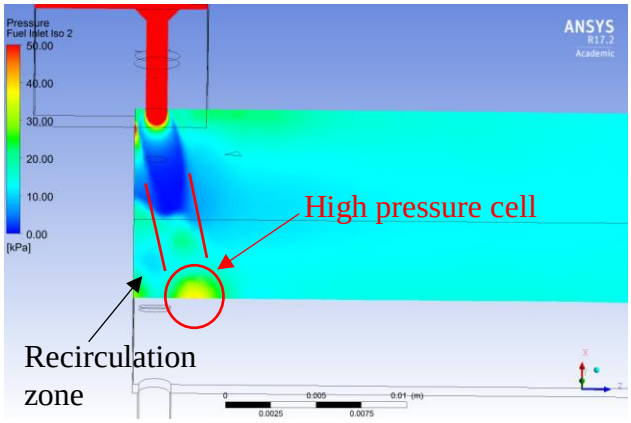

Figure 7.9. Pressure isosurface bisecting a fuel injector orifice

CHAPTER 8: CONCLUSIONS AND RECOMMENDATIONS

Not only did the CFD analysis offer a very plausible explanation for the aberrant sensor behavior, but it also did a magnificent job of helping to visualize the fluid flow within the mixing section of the combustor. It also offered additional explanations for phenomena previously thought to be unrelated to the injector behavior.

- Model results agreed with experimental data, validating the front end wall and side wall sensor data. The presence of recirculation zones near the front end wall is likely the reason for increased pressure readings at that location.
- Vortical entrainment of the gases was clearly visualized in the model solution. These vortices continued their behavior downstream, which will keep mixing the fuel and oxidizer before they reach the detonation zone. This efficient mixing will keep the required combustor length low, while eliminating the need for a pre-mixing chamber.
- The unexpected appearance of the recirculation zones also offered a possible explanation as to the extreme discoloration of the stainless steel on the combustor inner annulus wall. The same discoloration was also observed on the outer wall, but did not need additional explanation. Of course, this is speculative and requires validation.

While many questions were answered through the utilization of CFD analysis, many more were either unanswered or raised as a result of the work outlined in this paper. There is still much work that can be done in this area:

- Initiate simulations of multi-species flow and observe the effectiveness of mixing. This can lead to the prediction of the detonation zone, which can be proven or invalidated by experiment.
- Further refinement of the model by validating temperature readings, if possible.

- Addition of special considerations for the formation of a Mach disc within the injector plumes.
- Transient simulation of the fluids during each step in the firing sequence.
- Inclusion of detonation wave behavior, including compression and combustion of the products in the annulus.
- Given the results of these numerical simulations, installing a new pressure tap exactly between the O2 and H2 inlets in the RDE would offer a chance to further validate this model. This would also likely yield a more median front wall pressure value.

REFERENCES

Images

[i] https://bryanwweber.com/files/2012/01/Kailasanath_RDE.png

[ii] https://en.wikipedia.org/wiki/File:Fourier_series_and_transform.gif

Publications

[1] Boening, J. A., “Initiation of Orderly Spinning Detonation Waves via Phased Sparking”. Master’s Thesis. University of Washington, 2016. Print.

[2] Davidenko, D.M., Gökalp, I., Kudryavtsev, A.N., “Numerical Simulation of the Continuous Rotating Hydrogen-Oxygen Detonation with a Detailed Chemical Mechanism,” presented at West-East High Speed Flow Field Conference, Moscow, Russia, November 19-22, 2007.

[3] Kurosaka, M., Knowlen, C., Boening, J.A., “Theoretical and Experimental Consideration of the Continuous Rotating Detonation Engine”, AIAA Paper 2016-4967, July 2016.

[4] Nordeen, Craig A., "Thermodynamics of a Rotating Detonation Engine". Doctoral Dissertation. University of Conneticut, 2013. Web. <http://digitalcommons.uconn.edu/dissertations/277/>

[5] Boening, J.A., Heath, J.D., Byrd, T.J., Koch, J.V., Mattick, A.T., Bridenthal, R.E., Knowlen, C., and Kurosaka, M., “Design and Experiments of a Continuous Rotating Detonation Engine: a Spinning Wave Generator and Modulated Fuel-Oxidizer Mixing”, AIAA Paper 2016-4966, July 2016.

APPENDIX

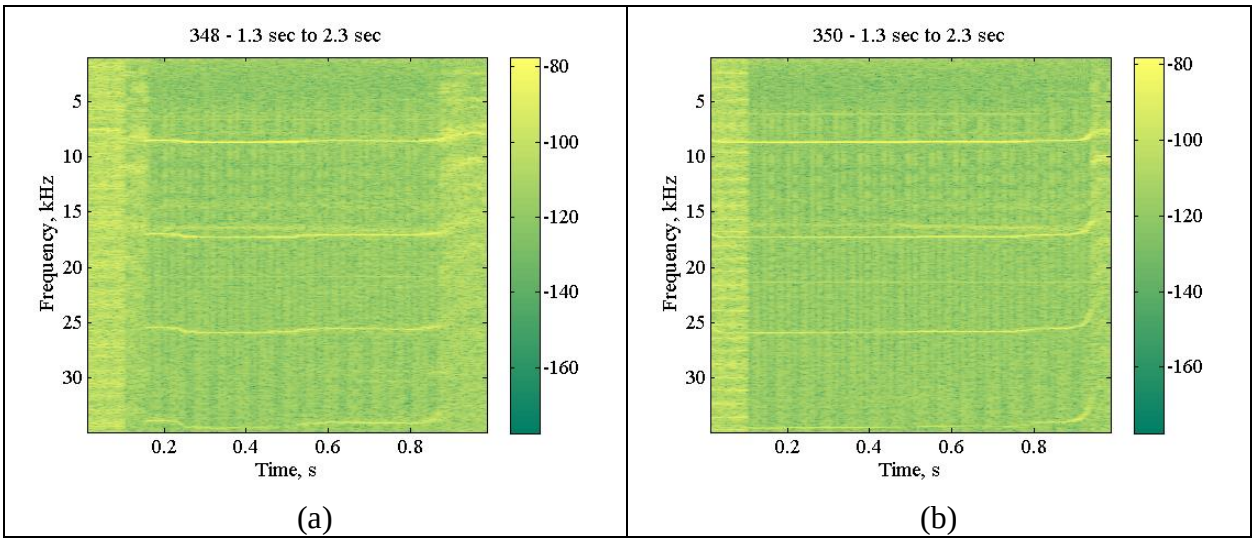

Figure A.1. Spectrogram plots from BFV settings at (a) 5.0 and (b) 6.0

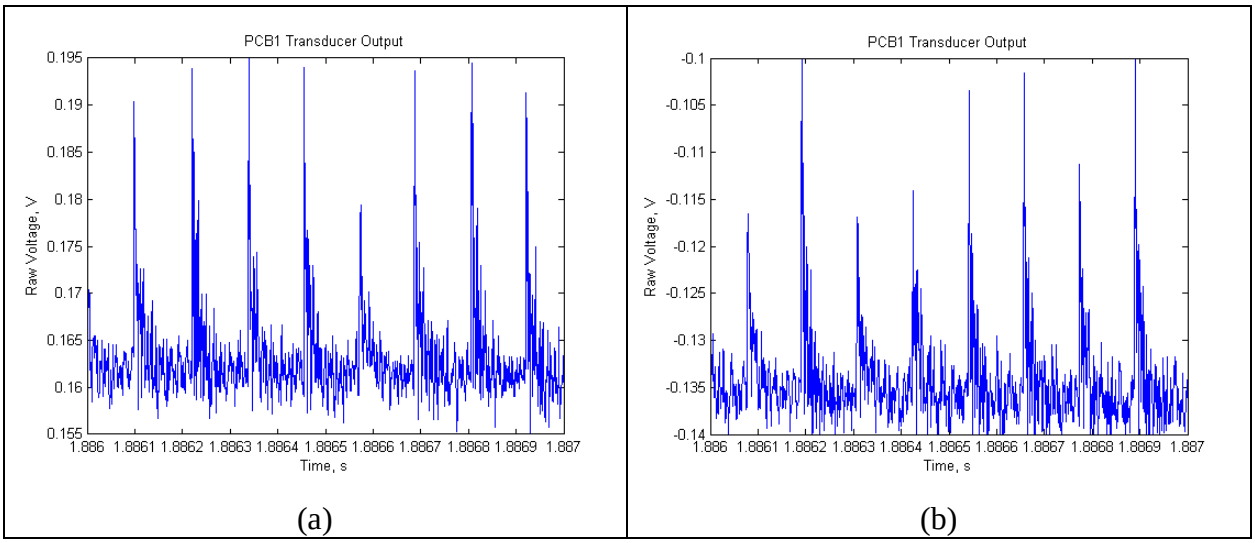

Figure A.2. Sample high-speed pressure transducer voltage output over time for BFV @ (a) 5.0 and (b) 6.0

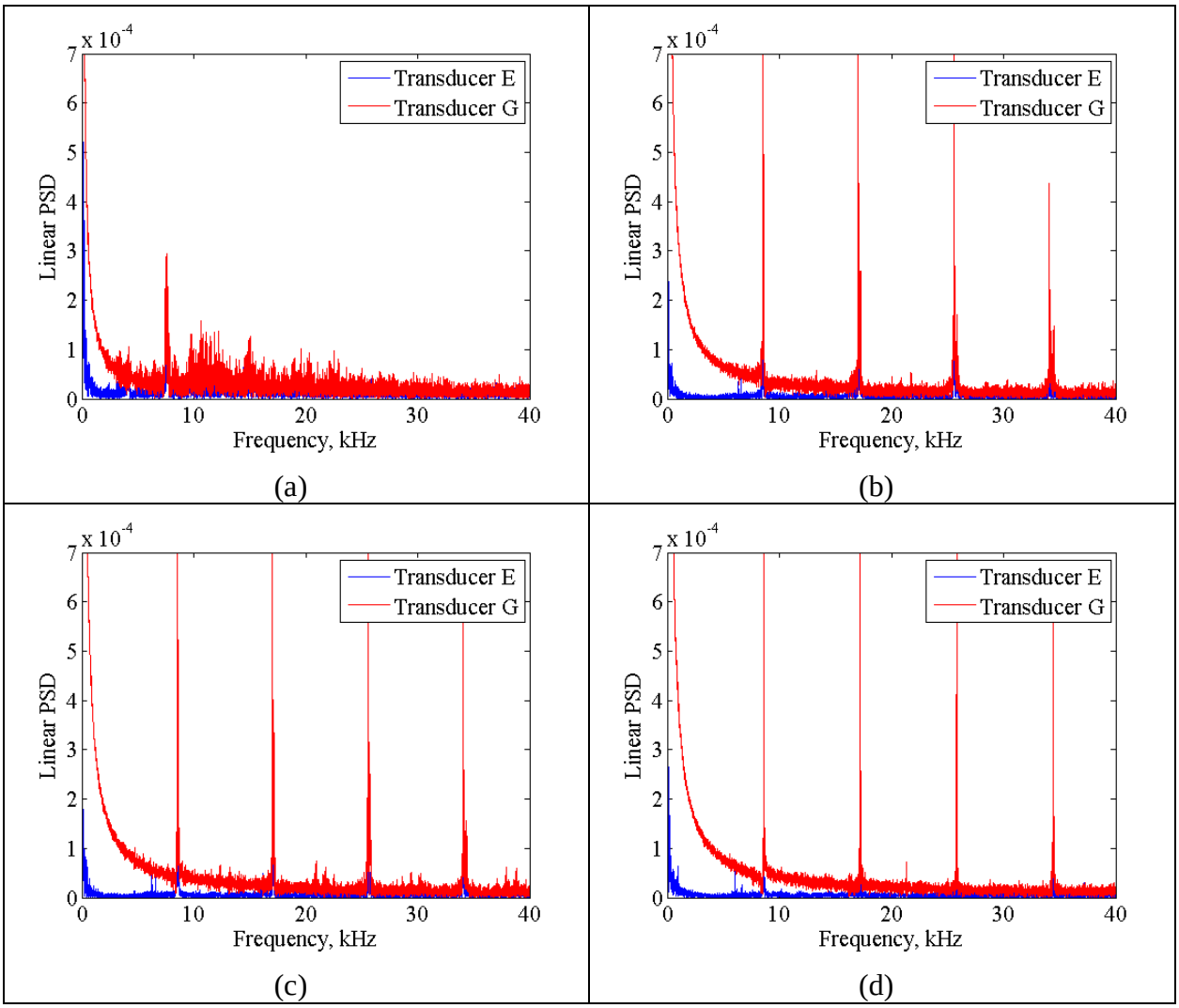

Figure A.3. Power spectral density vs. frequency of detonation activity for BFV @ (a) 4.5, (b) 5.0, (c) 5.5, and (d) 6.0

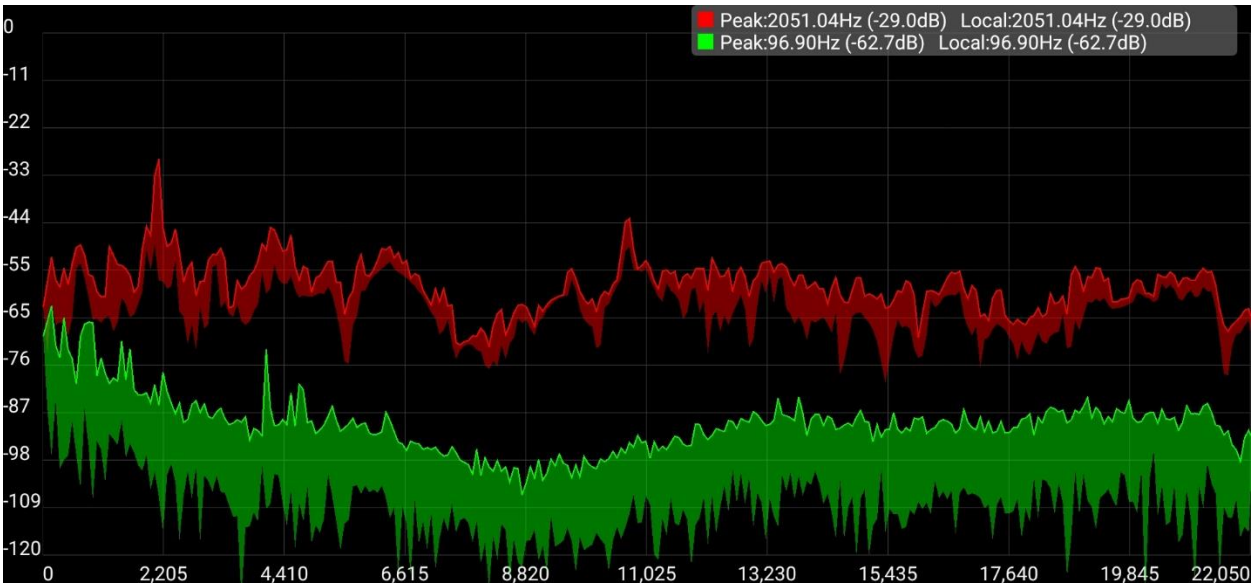

Figure A.4. Spectrum analysis of the airborne sound of a hammer striking the RDE, in red